# *CCDC151* Mutations Cause Primary Ciliary Dyskinesia by Disruption of the Outer Dynein Arm Docking Complex Formation

Rim Hjeij,[1,19] Alexandros Onoufriadis,[2,19,21] Christopher M. Watson,[3,4,19] Christopher E. Slagle,[5,19] Nikolai T. Klena,[6,19] Gerard W. Dougherty,[1] Małgorzata Kurkowiak,[1,7,8] Niki T. Loges,[1] Christine P. Diggle,[4] Nicholas F.C. Morante,[5] George C. Gabriel,[6] Kristi L. Lemke,[6] You Li,[6] Petra Pennekamp,[1] Tabea Menchen,[1] Franziska Konert,[9] June Kehlet Marthin,[10] Dorus A. Mans,[11,12] Stef J.F. Letteboer,[11,12] Claudius Werner,[1] Thomas Burgoyne,[13] Cordula Westermann,[14] Andrew Rutman,[15] Ian M. Carr,[4] Christopher O'Callaghan,[15,16] Eduardo Moya,[17] Eddie M.K. Chung,[18] UK10K Consortium, Eamonn Sheridan,[4] Kim G. Nielsen,[10] Ronald Roepman,[11,12] Kerstin Bartscherer,[9] Rebecca D. Burdine,[5] Cecilia W. Lo,[6] Heymut Omran,[1,20,*] and Hannah M. Mitchison[2,20]

A diverse family of cytoskeletal dynein motors powers various cellular transport systems, including axonemal dyneins generating the force for ciliary and flagellar beating essential to movement of extracellular fluids and of cells through fluid. Multisubunit outer dynein arm (ODA) motor complexes, produced and preassembled in the cytosol, are transported to the ciliary or flagellar compartment and anchored into the axonemal microtubular scaffold via the ODA docking complex (ODA-DC) system. In humans, defects in ODA assembly are the major cause of primary ciliary dyskinesia (PCD), an inherited disorder of ciliary and flagellar dysmotility characterized by chronic upper and lower respiratory infections and defects in laterality. Here, by combined high-throughput mapping and sequencing, we identified *CCDC151* loss-of-function mutations in five affected individuals from three independent families whose cilia showed a complete loss of ODAs and severely impaired ciliary beating. Consistent with the laterality defects observed in these individuals, we found *Ccdc151* expressed in vertebrate left-right organizers. Homozygous zebrafish *ccdc151*$^{ts272a}$ and mouse *Ccdc151*$^{Snbl}$ mutants display a spectrum of situs defects associated with complex heart defects. We demonstrate that *CCDC151* encodes an axonemal coiled coil protein, mutations in which abolish assembly of CCDC151 into respiratory cilia and cause a failure in axonemal assembly of the ODA component DNAH5 and the ODA-DC-associated components CCDC114 and ARMC4. *CCDC151*-deficient zebrafish, planaria, and mice also display ciliary dysmotility accompanied by ODA loss. Furthermore, CCDC151 coimmunoprecipitates CCDC114 and thus appears to be a highly evolutionarily conserved ODA-DC-related protein involved in mediating assembly of both ODAs and their axonemal docking machinery onto ciliary microtubules.

## Introduction

Ciliary motility plays a number of essential roles in the body.[1] Notably, coordinated cilia-based fluid movement across the multiciliated epithelial cell surface of respiratory airways forms the major host-defense mechanism of mucociliary clearance. Cerebrospinal fluid flow in the central nervous system is regulated by cilia lining the ventricles, and in the reproductive system, fallopian tube cilia assist propulsion of eggs toward the uterus. Sperm flagella, highly structurally related to cilia, drive male gamete motility. Motile cilia function in early embryogenesis to create a leftward nodal flow in or across vertebrate left-right organizers, which is necessary for induction of an asymmetric gene

[1]Department of General Pediatrics, University Children's Hospital Muenster, 48149 Muenster, Germany; [2]Genetics and Genomic Medicine Programme, University College London (UCL) Institute of Child Health, London WC1N 1EH, UK; [3]Yorkshire Regional Genetics Service, St. James's University Hospital, Leeds LS9 7TF, UK; [4]Leeds Institute of Biomedical and Clinical Sciences, University of Leeds, St. James's University Hospital, Leeds LS9 7TF, UK; [5]Department of Molecular Biology, Princeton University, Washington Road, Princeton, NJ 08544, USA; [6]Department of Developmental Biology, University of Pittsburgh, Pittsburgh, PA 15201, USA; [7]International Institute of Molecular and Cell Biology, Trojdena 4, 02-109 Warsaw, Poland; [8]Department of Molecular and Clinical Genetics, Institute of Human Genetics, Polish Academy of Sciences, Strzeszynska 32, 60-479 Poznan, Poland; [9]Max Planck Research Group on Stem Cells & Regeneration, Max Planck Institute for Molecular Biomedicine, and Medical Faculty, University of Muenster, 48149 Muenster, Germany; [10]Danish PCD Centre and Pediatrics Pulmonary Service, Department of Pediatrics and Adolescent Medicine, Copenhagen University Hospital, Rigshospitalet, 2100 Copenhagen, Denmark; [11]Department of Human Genetics, Radboud University Medical Center, PO Box 9101, 6500 HB Nijmegen, the Netherlands; [12]Radboud Institute for Molecular Life Sciences, Radboud University Nijmegen, PO Box 9101, 6500 HB Nijmegen, the Netherlands; [13]UCL Institute of Ophthalmology, 11–43 Bath Street, London EC1V 9EL, UK; [14]Gerhard-Domagk-Institut for Pathology, University Children's Hospital Muenster, 48149 Muenster, Germany; [15]Centre for PCD Diagnosis and Research, Department of Infection, Immunity and Inflammation, RKCSB, University of Leicester, Leicester LE2 7LX, UK; [16]Respiratory, Critical Care & Anaesthesia, Institute of Child Health, University College London & Great Ormond Street Children's Hospital, 30 Guilford Street, London WC1N 1EH, UK; [17]Bradford Royal Infirmary, Bradford, West Yorkshire BD9 6R, UK; [18]General and Adolescent Paediatrics Section, Population, Policy and Practice Programme, University College London (UCL) Institute of Child Health, London WC1N 1EH, UK
[19]These authors contributed equally to this work
[20]These authors contributed equally to this work in a supervisory role
[21]Present address: Department of Medical and Molecular Genetics, Division of Genetics and Molecular Medicine, King's College London School of Medicine, Guy's Hospital, London SE1 9RT, UK
*Correspondence: heymut.omran@ukmuenster.de
http://dx.doi.org/10.1016/j.ajhg.2014.08.005. 

expression cascade in the lateral plate mesoderm that determines left-right organ asymmetry (situs).[2]

Motile cilia and sperm flagella extend from the cell body containing a 9+2 axonemal arrangement of two central microtubules and nine peripheral microtubule doublets, except in nodal monocilia, which lack the central microtubule pair (9+0). Microtubule-attached dynein arm motors, radial spokes, and nexin-dynein regulatory complexes arranged with regular periodicity along the peripheral microtubules provide a rigid structure and the biophysical force for ciliary beating. The beat is generated by coordinated sliding of adjacent microtubule doublets, powered via dynein-arm-driven ATP hydrolysis. This axonemal architecture is highly conserved in evolution and is found in the biflagellate alga *Chlamydomonas reinhardtii* as well as humans, where flagellar/ciliary dyneins make up two distinct structures, the outer dynein arms (ODAs) and the inner dynein arms (IDAs), each anchored to a specific site on the A-tubule of the doublet microtubules. The ODAs, with a regular spacing of 24 nm along the axonemal microtubules, contribute as much as four-fifths of the sliding force needed for flagellar/ciliary bending.[3]

Primary ciliary dyskinesia (PCD [MIM 244400])[4,5] refers to an autosomal-recessive inherited disorder in which structure and assembly of motile cilia and sperm is deficient, often accompanied by visible ultrastructural defects, resulting in dysmotile or static axonemes. PCD is characterized by lifelong recurrent respiratory infections and irreversible, destructive airway disease (bronchiectasis) of early onset. Otitis media and nasal polyps are common and male infertility may occur, as well as laterality defects affecting approximately half of affected individuals, with around 12% manifesting as complex isomerisms and heterotaxies usually associated with congenital heart defects.[6,7] Distinct from ultrastructural ciliary defects, *CCNO* (MIM 607702) mutations have recently been identified to cause a mucociliary clearance disorder related to, but distinct from, PCD that was previously called ciliary aplasia but is now termed RGMC (reduced generation of multiple motile cilia), because in RGMC a few motile cilia are still detectable at the cell surface.[8]

An estimated 70%–80% of PCD cases involve deficiency and loss of the ciliary outer dynein arms, with around a quarter of that total also involving inner dynein arm loss.[9,10] Of 28 genes previously reported to have causative mutations for PCD,[11,12] 8 encode proteins of the ODAs or the ODA docking complex system (ODA-DC) (*DNAH5* [MIM 603335], *DNAH11* [MIM 603339], *CCDC114* [MIM 615038], *DNAL1* [MIM 610062], *DNAI1* [MIM 604366], *DNAI2* [MIM 605483], *NME8* [MIM 607421], and *ARMC4* [MIM 615408]),[13–21] mutations of which generally cause isolated outer dynein arm deficiency. Ten genes encode cytoplasmic proteins involved in assembly and transport of the dynein arms into axonemes (*SPAG1* [MIM 603395], *DNAAF1* [MIM 613190], *DNAAF2* [MIM 612517], *HEATR2* [MIM 614864], *DNAAF3* [MIM 614566], *DYX1C1* [MIM 608706], *ZMYND10* [MIM 607070], *LRRC6* [MIM 614930], *C21orf59* [MIM 615494], and *CCDC103* [MIM 614677]),[22–32] mutations of which cause combined outer and inner dynein arm deficiency. Eight other genes with causal mutations are components or associated factors of the nexin-dynein regulatory complexes (*CCDC39* [MIM 613798], *CCDC40* [MIM 613799], *CCDC65* [MIM 611088], and *DRC1* [previously known as *CCDC164*] [MIM 615288]),[31,33–35] radial spokes (*RSPH1* [MIM 609314], *RSPH4A* [MIM 612647], and *RSPH9* [MIM 612648]),[11,36] or central pair microtubules (*HYDIN* [MIM 610812]).[37] Syndromic PCD with retinitis pigmentosa and developmental disorders can be caused by *RPGR* (MIM 312610) or *OFD1* (MIM 300170) mutations[38,39] and is characterized by X-linked transmission.

Although much progress in gene identification for PCD has been achieved, it has been recently estimated that the known genes in which mutations cause PCD account for about 65% of PCD cases.[40] Therefore, we employed a next-generation sequencing (NGS) approach for linkage mapping and variant identification in order to identify additional PCD-causing mutations. This analysis revealed loss-of-function mutations in *CCDC151* in three unrelated families characterized by PCD with specific loss of the ODAs. By analyzing CCDC151-deficient human cells, mice, and zebrafish, we show a requirement for CCDC151 in the correct establishment of left-right asymmetry because loss of CCDC151 function is associated with the randomization of visceral organ positioning. A severe reduction of CCDC151 occurs in the axonemes of nasal respiratory cilia of individuals carrying *CCDC151* nonsense mutations, which disrupts assembly of both the ODAs and the ODA targeting and docking components CCDC114 and ARMC4 into axonemes. These results highlight the essential role of CCDC151 in the specification of ciliary motility during human and vertebrate development.

## Material and Methods

### Subjects

Individuals included in the study had a clinical diagnosis of PCD confirmed by standard clinical diagnostic criteria documenting typical symptoms of neonatal respiratory distress and chronic respiratory disease features including rhinosinusitis, airway infections and fluid congestion, otitis media, and bronchiectasis.[41] Clinical test results included medical imaging (X-ray); light, electron, and immunofluorescence microscopy to detect ciliary motility and analyze ciliary structure; and nasal nitric oxide measurements. For studies of affected individuals and their families, signed and informed consent was obtained from all participants prior to history recording, blood drawing, and nasal biopsy, using protocols approved by the Institutional Ethics Review Board of the University of Muenster (Germany), the Institute of Child Health/Great Ormond Street Hospital, London (UK) (#08/H0713/82), and collaborating institutions.

### Genetic Analysis

Next-generation sequencing was performed either by whole-exome sequencing using the SureSelect v.5 (no UTRs) exome

reagent (Agilent Technologies) with variant filtering performed using the AgileExomeFilter program as previously reported[42] or by a targeted panel-based resequencing of selected candidate genes using SureSelect RNA baits designed with the SureSelect Target Enrichment protocol (Agilent SureDesign wizard, Agilent Technologies) with filtering as previously reported.[11] Sequencing was performed on a HiSeq 2500 in rapid run mode or HiSeq 2000 (Illumina). Sanger sequencing was performed to screen or confirm *CCDC151* mutations in affected individuals and in other family members for segregation analysis, and details of the sequencing primers used are available on request.

Homozygosity mapping in family 71154 used either the whole-exome sequence data for affected individual 71154 II:2 or SNP genotyping data generated using the Affymetrix Genome-Wide Human SNP Array v.6.0 (Affymetrix) in both siblings 71154 II:1 and II:2. AgileMultiIdeogram, which is based on a previously published method[43] modified to use software NGS-generated VCF rather than SAM files, was used to generate a visual output plus numerical chromosomal coordinates for autozygous regions of interest.

### Mapping, Sequencing, and Genotyping the *flanders* Locus

The *flanders* locus was mapped to chromosome 6 of the zebrafish genome using a genome-wide panel of SSLP markers for low-resolution mapping. Finer mapping using additional SSLP markers placed *flanders* in a 2.4 Mb region defined by markers z17212 and z6601. The *flanders* c.631T>A mutation destroys a DraI site and this was used to create a genotyping screen employing the primers listed in Table S1 available online. The wild-type amplicon cut by DraI produces a 159-bp band; the mutant amplicon not cut by DraI is 213 bp long.

### Zebrafish Microinjections

In vitro transcribed mRNAs were generated from linearized plasmid templates using the mMessage mMachine SP6 transcription kit (Ambion #AM1340) from pCS2-*ccdc151* plasmid. Translation-blocking morpholinos for *ccdc151* (5′-AGACCGAC GTGCCGGGCATTATATA-3′) were designed by Gene Tools, and mRNAs were diluted in 10 mg/ml Phenol Red and injected in 500 pl drops into the yolks of 1- to 4-cell-stage embryos.

### Zebrafish Microscopy

Live embryo and in situ hybridization images were captured at 4× or 10× magnifications using a ProgressC14 digital camera (Jenoptik) on a Leica MZFLIII microscope. Brightfield video microscopy of Kupffer's vesicle and embryonic kidneys was performed on an inverted Leica SP5 spectral confocal microscope. Live embryos were mounted in 2% low-melt agarose in glass-bottom tissue culture dishes and illuminated with 561 nm wavelength light. Recordings were captured at 170 frames/s using a 63× glycerin immersion objective and beat frequency was analyzed as described.[44] Histology of zebrafish embryos was performed as described.[45]

### Recovery of *Ccdc151*$^{Snbl}$ Mouse Mutation by Whole-Mouse Exome Sequencing Analysis

The pathogenic mutation in the *Snowball* ENU mutant (b2b1885Clo, MGI 5445347) was identified by whole mouse exome sequence capture performed using the Agilent SureSelect Mouse All Exon V1 kit followed by pair-end sequencing using an Illumina HiSeq 2000 sequencer. Average 51.8× target coverage was achieved. Reads were mapped to the C57BL/6 reference genome (mm9) using CLCBio Genomic Workbench and GATK v.2.8 software. Sequence variants were annotated with Annovar and filtered against dbSNP and our in-house mouse exome databases with custom scripts. Five homozygous coding variants were obtained in the single homozygous *Snbl* mutant analyzed by exome sequencing analysis. Genotyping for all five coding variants in two additional *Snbl* mutants exhibiting heterotaxy or situs inversus totalis identified only a c.828+2T>C *Ccdc151* variant as consistently homozygous in all of the *Snbl* mutant offspring. This was further confirmed with additional breeding and genotyping/phenotyping analysis.

### *Ccdc151* Transcript Analysis in *Ccdc151*$^{Snbl}$ Mutant Trachea

Total RNA was isolated from mouse trachea using the RNeasy Plus Micro Kit (QIAGEN). cDNA was synthesized from 2 μg of total RNA and PCR amplified using AmpliTaq Gold DNA polymerase (Life Technologies) using cycle parameters: 95°C for 5 min, followed by 40 cycles at 95°C for 30 s, 58°C for 30 s, and 72°C for 1 min, then 72°C for 5 min. Products were analyzed by agarose gel electrophoresis. Five primer pairs were used for PCR amplification to interrogate the *Ccdc151* transcript and *Dnah5* was also amplified as a positive control (primers are listed in Table S1).

### Whole-Mount In Situ Hybridization

For mouse analysis, CD-1 mouse embryos were collected after timed mating between embryonic day (E) 7.5 and E8.0 following standard procedures. Midday on the day of plug detection was defined as 0.5 dpc. In addition, embryos were staged by somite counting. Sense and antisense probes for *Ccdc151* were made from a 709 bp pCRII-TOPO construct (RefSeq accession number NM_001163787.1, nt 1031–1740, transcript variant 1) made by TOPO TA cloning (Invitrogen) after amplification from complementary DNA. Probes were synthesized with digoxigenin NTPs (Roche) after template linearization with HindIII (sense) or NotI (antisense) before RNA synthesis with T7 or SP6 RNA polymerases, respectively. For whole-mount in situ hybridization, staged embryos were fixed overnight at 4°C in 4% paraformaldehyde in 1× PBS. Whole-mount in situ hybridization (WISH) was then performed according to standard procedures with minor modifications.[27] Stained samples were transferred into 80% glycerol, and images were captured using a Scion CFW-1310C color digital camera mounted on an Axioskop 2 plus microscope (Zeiss) and Image-Pro Express.

For zebrafish analysis, the full-length *ccdc151* cDNA (GenBank ID BC124606.1, Open Biosystems) was cloned using standard methods into pCS2 for sense and antisense probe transcription, with RNA probes transcribed from linearized plasmid templates using DIG-labeled nucleotides and used in a standard WISH protocol. *Southpaw* expression was investigated as previously described.[46]

### Immunofluorescence Analysis

Respiratory epithelial cells were obtained by nasal brush biopsy (Engelbrecht Medicine and Laboratory Technology, Germany) and suspended in cell culture medium. For mouse tracheal samples, freshly harvested trachea were placed in L-15 media (Life-Technologies, 21083-027) and scraped with a Rhino-Probe Curette (LabPlanet, SY-96-0925). Samples were spread onto glass slides,

air-dried, and stored at −80°C until use. Cells were treated with 4% paraformaldehyde, 0.2% Triton X-100, and 1% skimmed milk prior to incubation with primary (2–3 hr at room temperature or overnight at 4°C) and secondary (30 min at room temperature) antibodies. Appropriate controls were performed by omitting the primary antibodies. Polyclonal rabbit anti-DNALI1 and anti-DNAH5 were reported previously,[19] as well as the mouse monoclonal anti-GAS8.[34] Monoclonal mouse anti acetylated-α-tubulin (T7451) and polyclonal rabbit anti-ARMC4 (HPA037829) were obtained from Sigma. Polyclonal rabbit anti-CCDC114 (HPA042524) and anti-CCDC151 (HPA044184) were obtained from Atlas Antibodies. Anti-mouse Alexa Fluor 488 and anti-rabbit Alexa Fluor 546 were used as secondary antibodies (Molecular Probes, Invitrogen). DNA was stained with Hoechst 33342 (Sigma). Immunofluorescence (IF) images were taken with a Zeiss Apotome Axiovert 200 and processed with AxioVision v.4.8 and Adobe Creative Suite 4. Mouse IF images are 3D reconstructions of z-stacks made with the Apotome.

### Cilia Transmission Electron Microscopy and Motility

Human TEM and high-speed video microscopy using the SAVA system were performed as previously reported.[19,42] TEM in mice and zebrafish was prepared as previously reported,[11] and video microscopy was performed as previously reported.[44,47–49]

### cDNA Cloning

*CCDC114* and *CCDC151* were cloned by nested PCR from human bronchial epithelial cell cDNA (ScienCell, cat no. 3214) using KOD polymerase according to manufacturer's directions and recombined with pDONR201 Gateway vector via BP Clonase II reaction.

Subsequently, *CCDC114* and *CCDC151* were subcloned into myc and 3× FLAG epitope-tagged Gateway destination vectors via LR Clonase reaction. All cDNA clones were confirmed by sequence analysis and matched RefSeq gene accession number NM_144577.3 (*CCDC114*) or NM_145045.4 (*CCDC151*).

The primers used for cDNA cloning are listed in Table S1.

### Coimmunoprecipititation and Immunoblotting

HEK293 cells were transfected with plasmids encoding myc- and FLAG-tagged cDNA constructs using Gene Juice (Novagen) at approximately 0.1 μg DNA per ml of media. Within 24 hr, cells were collected in 1× PBS and lysed in 1 ml of the following buffer: 50 mM Tris-Cl (pH 8.0), 150 mM NaCl, 1% IGEPAL, 0.5 mM EDTA, and 10% glycerol supplemented with protease (Roche Complete) and phosphatase inhibitors (Cocktails 2 and 3, Sigma Aldrich). Lysates were centrifuged at 16,000 × *g* for 30 min at 4°C. Approximately 2 mg of each lysate was precleared with 4 μg of rabbit control IgG antibody for 2 hr at 4°C and then incubated with MagSi/protein A beads (MagnaMedics, Germany) for 1 hr. Lysates were then incubated with either 2 μg of rabbit anti-CCDC114 or anti-CCDC151 antibody and 2 μg of control IgG antibody overnight at 4°C, and then incubated with MagSi/protein A beads for 1 hr to capture immunoprecipitates. Bead complexes were washed four times in lysis buffer and then resuspended in 1× LDS buffer supplemented with DTT and heated for 10 min at 90°C. Lysates were electrophoresed in NuPAGE 4%–12% Bis-Tris gels, transferred to PVDF filters, and subsequently immunoblotted with either anti-myc (A.7) or anti-FLAG (M2) mouse monoclonal antibodies. PVDF filters were washed three times in TBS-T (10 min each) before blocking in 5% BSA for 2 hr at room temperature. Filters were then washed three times (10 min each) before incubation with primary antibody (diluted in TBS-T) overnight at 4°C. Filters were washed three times (10 min each) and then incubated with goat anti-mouse HRP secondary antibody for 1 hr at room temperature. Filters were then washed four times and developed by ECL using Prime Western Blotting Detection Reagent (Amersham). Images were digitally acquired using a FUSION-SL Advance Imager (PeqLab) and modified for contrast using Adobe Photoshop v.CS4. All wash and incubation steps were performed with gentle shaking. The following antibodies were used: rabbit polyclonal anti-CCDC151 (Atlas Antibodies, HPA044184), rabbit polyclonal anti-CCDC114 (Atlas Antibodies, HPA042524), mouse monoclonal anti-myc (1:2,000; clone A.7, Abcam), rabbit polyclonal control IgG (sc-2027, Santa Cruz), mouse monoclonal anti-FLAG (1:2,000; clone M2, Sigma Aldrich), and goat anti-mouse HRP antibody (1:5,000; NA931V, GE Healthcare).

### Yeast Two-Hybrid Analysis

Direct interaction between CCDC114 and CCDC151 was tested as previously described.[27]

## Results

### Identification of *CCDC151* Mutations through High-Throughput Autozygosity Mapping and Sequencing

We used a high-throughput next-generation sequencing (NGS) approach to identify PCD-causing mutations in affected individuals that were clinically diagnosed with PCD caused by deficiency of the axonemal ODAs. The NGS pipeline consisted of either whole-exome sequencing or a targeted panel-based resequencing of selected candidate genes, performed in two separate cohorts of individuals with PCD as previously reported.[11,42] NGS data were processed through standard quality controls, and sequence reads were aligned back to the genome and annotated for DNA variants, which were then filtered according to a rare recessive disease model[11,42] (Tables S2 and S3). This excluded genes that did not have at least one homozygous or two heterozygous changes that were either previously unreported or occurring with an estimated frequency of less than 0.01 in publically available human exome databases (1000 Genomes, NHLBI EVS, dbSNP139). All variants except those predicted to produce a nonsynonymous or splice-site substitution, or an indel, were then removed. For the cases processed through exome sequencing, a filter was also applied to remove variants that were not in chromosomal regions of interest highlighted by autozygosity mapping.

In both the resequencing panel and exome-sequence analysis, all variants meeting the filtering criteria were finally examined to identify those present in genes predicted to have motile cilia function. From gene panel analysis that was conducted on 70 affected individuals, this revealed a homozygous single-base substitution in *CCDC151* (RefSeq NM_145045.4), c.925G>T, predicting a premature termination of translation p.Glu309*, in a Bedouin-Arabic individual (UCL-65 II:8). The NGS sequence filtering steps taken to reveal this predicted loss-of-function variant as the likely disease cause are shown

in Table S2. Individual UCL-65 II:8 also carries a single heterozygous variant in *DNAH2* (rs7601298) and a homozygous variant in *DNAH3* (rs138753702), which are predicted to be damaging to protein function, but these genes encode inner arm dyneins.[50] These and a homozygous *CCDC40* variant (rs10693712), described fully in Table S2, were not considered a possible cause of outer dynein arm loss and furthermore were excluded as causal by segregation analysis. The other variant meeting the filtering criteria was *CCDC151* c.925G>T (p.Glu309*), which was also the only biallelic stop-gain mutation detected.

In the exome analysis that was conducted on 28 affected individuals, an autozygosity linkage mapping approach was employed in consanguineous families as an extra filter to analyze sequence variants in a narrowed set of chromosomal regions of interest. Genome-wide SNP genotyping (Affymetrix human SNP Array v.6.0) identified regions of homozygosity unique to the affected sibling in one UK-based consanguineous family of Pakistani origin (71154). We compared these data to SNP mapping data that could be derived from exome sequencing, to assess its utility for genetic mapping. We found that the information derived from both data sets was almost identical, identifying 15 autozygous regions of interest totalling 177 Mb unique to the affected sibling 71154 II:2, including a large autozygous region on chromosome 19p13 containing *CCDC151* (Figure S1). A homozygous *CCDC151* single-base substitution c.1256C>A was identified in individual 71154 II:2 on the basis of prioritizing these linked regions, predicting a premature termination of translation p.Ser419* (Figures 1A and 1B). The NGS sequence filtering steps applied in family 71154 are summarized in Table S3.

Familial segregation analysis performed in available family members showed the *CCDC151* variant inheritance pattern to be consistent for an autosomal-recessive disease in both families, including in a second affected sibling (UCL-65 II:7) (Figure 1A). This approach to derive autozygosity linkage mapping data from polymorphic markers and then focus on linkage-positive regions to identify rare disease-causing variants is powerful for exome-based gene discovery in consanguineous families, potentially removing the need for the extra cost of SNP array analysis in such families. Exome-sequencing-based linkage mapping has previously been tested for PCD[51] and has proven successful for other genetic conditions.[52]

CCDC151 is the vertebrate ortholog of *Chlamydomonas reinhardtii* ODA10, which was recently shown to be required for ODA assembly in these ciliated algae.[53] We therefore considered *CCDC151* a reasonable PCD candidate gene and proceeded to screen for *CCDC151* mutations by Sanger sequencing in 150 additional affected individuals with ODA defects documented either by transmission electron microscopy (TEM) or by immunofluorescence analysis (IF). After PCR amplification and sequence analysis of all 13 exons, we identified *CCDC151* mutations in individual OP-675, who carried the same homozygous nonsense mutation found in family UCL-65 (c.925G>T [p.Glu309*]). Familial segregation confirmed that this variant again segregated with the disease status in the wider family, including in another affected sibling, OP-1255 (Figure 1A). Neither of the two variants identified in this study, c.925G>T (p.Glu309*) or c.1256C>A (p.Ser419*), is present in the 1000 Genomes or Exome Variant Server databases.

In total, the mutational analysis detected *CCDC151* loss-of-function nonsense mutations affecting five PCD individuals in three families. All the affected individuals displayed a clinical phenotype consistent with PCD including recurrent upper and lower airway disease with chronic respiratory symptoms and bronchiectasis, as well as nasal blockages, polyps, and otitis media. In all but one affected person, there was very early involvement with neonatal respiratory distress syndrome (Table S4). Four of the five affected individuals had laterality defects (Figure 1C, Table S4), with a congenital cardiac defect documented in individual OP-675 who had a ventricular septal defect (VSD). These clinical findings suggest that *CCDC151* deficiency causes PCD and that CCDC151 function is required for correct laterality determination, which is consistent with the known role of ODA-generated ciliary motility in determining situs-specific morphogenesis.[6]

Previous studies supporting our human genetic data have shown that the *Chlamydomonas* CCDC151 ortholog ODA10 is a constituent of the flagella axoneme and is also present in the cell body.[53] The null mutant *oda10* *Chlamydomonas* strain lacks outer dynein arms, and *ccdc151* deficiency in zebrafish knockdown morphants also causes a specific loss of ODAs.[54] Human *CCDC151* encodes a protein of 595 amino acids, and we used SMART to detect its domains, confirming that human CCDC151 is predicted to have three highly conserved coiled-coil domains. Coiled-coil domains are present in numerous proteins of diverse function and are recognized for their abundance in transcription factors involved in cell growth and proliferation and for their role in mediating interactions with other proteins.[55] The *CCDC151* mutations we identified in the PCD families are both predicted to cause premature protein truncations located within coiled-coil domains and would likely disrupt protein function (Figure 1D).

### *ccdc151* Is Mutated in the Zebrafish *flanders* Mutant, Leading to Ciliary Defects Including Laterality Defects

The evolutionarily conserved role of CCDC151 in vertebrate cilia was verified by examination of zebrafish *flanders* mutants. *ccdc151*$^{ts272a}$ (*flanders*) was generated in the Tübingen ENU mutagenesis screen.[56] *flanders* mutants present morphologically with a ventral body curvature and kidney cysts (Figure 2A), characteristic of mutations that affect ciliary motility in zebrafish. We mapped the *flanders* mutation to a 2.4 Mb region on chromosome 6 and sequenced exons from candidate genes in this region. A c.631T>A substitution was discovered in exon 6 of *ccdc151* (RefSeq NM_001077369.2) that is predicted to introduce a premature stop codon at lysine 211 of the

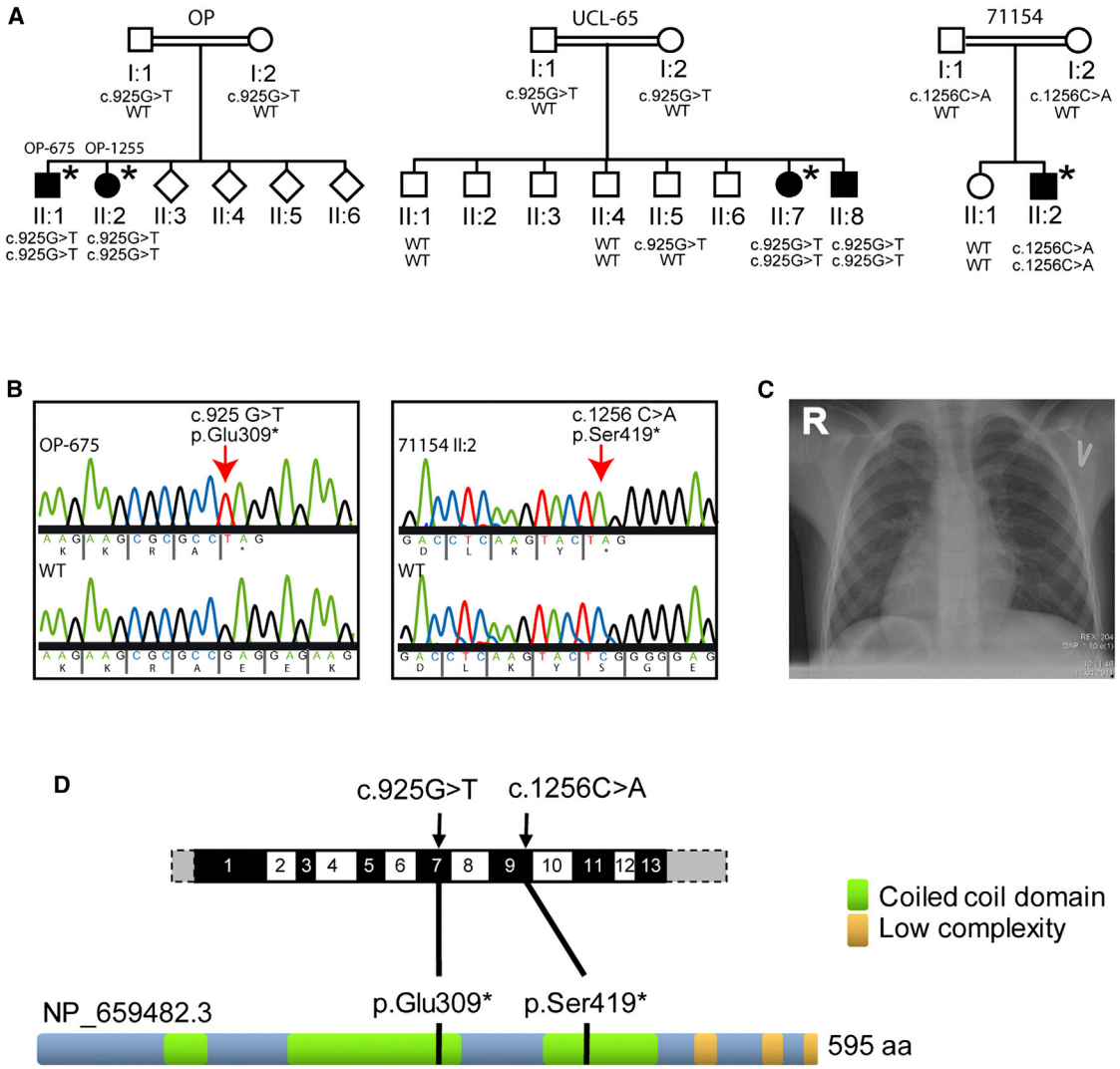


**Figure 1. *CCDC151* Recessive Loss-of-Function Mutations in Three Families with Primary Ciliary Dyskinesia and Situs Inversus**
(A) Pedigree structure and segregation analysis in PCD families carrying *CCDC151* mutations showing an inheritance pattern consistent with disease status, as indicated by presence of the mutant or normal (WT) alleles. Consanguineous unions OP and UCL-65 share the same mutation, c.925G>T. Asterisks indicate situs inversus; double lines indicate first-degree consanguinity.
(B) Representative sequence traces (top) for the two *CCDC151* homozygous nonsense mutations detected in affected individuals. The examples are amplified from individual OP-675 (c.925G>T) predicting a premature termination of translation p.Glu309* and individual 71154 II:2 (c.1256C>A) predicting a premature termination of translation p.Ser419*. The normal (WT) sequence is shown below.
(C) Chest X-ray of individual OP-675 shows situs inversus totalis; R indicates right side.
(D) The location of mutations within the intron-exon structure of *CCDC151* is shown above: black and white boxes indicate the coding exons, gray the 5′ and 3′ UTRs. Below, the location of the mutations is shown within the corresponding 595-amino-acid CCDC151 protein (RefSeq NP_659482.3) model, predicted using SMART. Green boxes indicate coiled-coil domains; yellow boxes indicate low-complexity repeat regions.

545 amino acid protein (p.Lys211*) (Figure 2B). Consistent with what was previously reported,[54] whole mount in situ hybridization (WISH) analysis identified *ccdc151* expression restricted to tissues that contain motile cilia in zebrafish including the left-right organizer (Kupffer's vesicle [KV]), the otic vesicle, and the pronephric tubules (Figure 2C). Further support that *ccdc151* is the gene mutated in *flanders* was provided by in situ hybridization showing evidence for nonsense-mediated decay of the transcript in embryos genotyped as mutant, which entirely lacked expression (Figure 2D). In addition, the *flanders* phenotype could be rescued by injection of *ccdc151* RNA (Figure S2), and a phenocopy of the *flanders* mutant phenotype was generated by antisense morpholino injection (Figures S2 and S3).

To examine left-right patterning in *flanders* mutants and *ccdc151* morphants, expression of the nodal gene *southpaw* (*spaw*) and the positioning of the visceral organs (heart, liver, and pancreas) were examined (Figure S3). Whereas wild-type siblings express *spaw* in the left lateral plate mesoderm and display situs solitus, *flanders* mutant embryos and *ccdc151* morphants show randomization of *spaw*

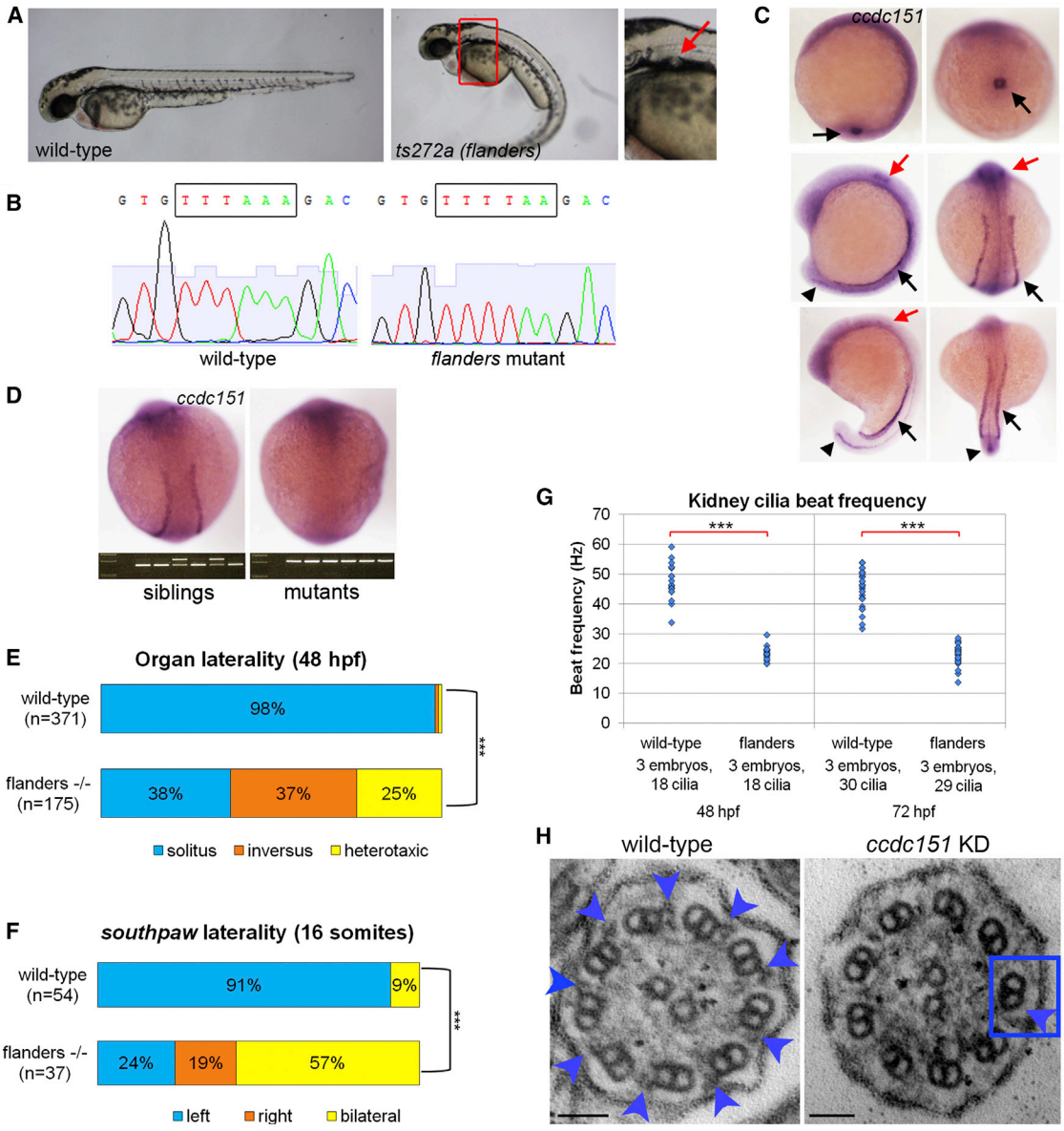


**Figure 2. Zebrafish *ccdc151* Is Expressed in Ciliated Tissues and Required for Ciliary Motility-Dependent Processes**

(A) Wild-type (left) and *flanders* (*ts272a*) mutant (center and right) zebrafish embryos at 48 hr postfertilization (hpf). Right panel is a magnification of the boxed region in the center panel. Red arrow indicates pronephric cysts evident in *flanders* mutants.

(B) DNA sequencing chromatograms demonstrating the *ccdc151* c.631T>A (p.Lys211*) nonsense mutation in *flanders* mutants.

(C) In situ hybridization demonstrating wild-type *ccdc151* expression in Kupffer's vesicle at tailbud stage (black arrows, top panels) and intermediate mesoderm (black arrows), otic vesicles (red arrows), and neural tube (black arrowheads) during early (10 somites; middle panels) and late (20 somites; bottom panels) somitogenesis.

(D) In situ hybridization demonstrating loss of *ccdc151* expression in *flanders* mutants. Progeny of *flanders*/+ incrosses were sorted based on *ccdc151* expression and genotyped using the DraI restriction site destroyed by the c.631T>A (p.Lys211*) mutation.

(E) Quantification of asymmetric organ positioning in embryos at 48 hpf. *flanders* mutants and siblings were sorted based on body curvature morphology prior to in situ hybridization. ***chi-square p value $< 10^{-55}$.

(F) Quantification of asymmetric expression of zebrafish *nodal* homolog *Southpaw* during somitogenesis. *flanders* mutants and siblings were distinguished based on DraI restriction site presence or absence following in situ hybridization. ***chi-square p value $< 10^{-9}$.

(G) Quantification of pronephric cilia beat frequency in *flanders* mutants and siblings at 48 hpf and 72 hpf. ***Student's t test p value $< 10^{-16}$.

(H) Transmission electron microscopy of cross-sections through pronephric cilia reveals the lack of outer dynein arms in embryos injected with the *ccdc151* morpholino (KD = knockdown; blue box and arrow), compared to a wild-type uninjected embryo where outer dynein arms (blue arrows) are visible. Scale bars represent 50 nm.

expression, situs inversus, and heterotaxic organ placement (Figures 2E, 2F, and S3). To explore the effect in *flanders* mutants and *ccdc151* morphants on ciliary motility, cilia were imaged using high-speed videomicroscopy in the KV and developing kidney. In *flanders* mutants, cilia in the KV moved irregularly, occasionally switching direction, or

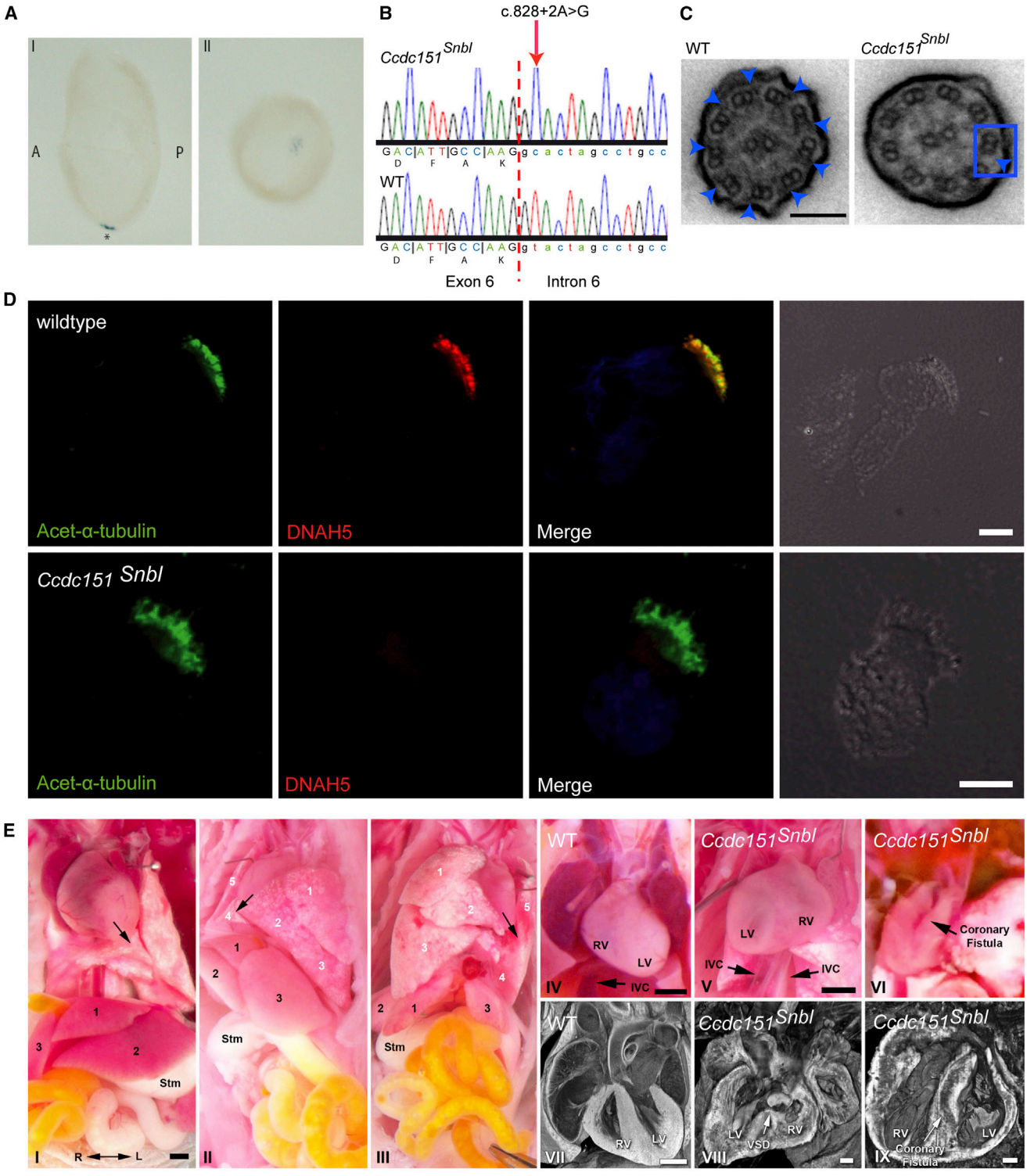


**Figure 3.** ***Ccdc151*** **Localizes to Embryonic Node Monocilia and** ***Ccdc151*** $^{Snbl}$ **Mutants Exhibit a Spectrum of Laterality Phenotypes Including Complex Congenital Heart Defects Associated with Heterotaxy**

(A) Whole-mount in situ hybridization analysis of *Ccdc151* in wild-type E7.5 mouse embryos shows that *Ccdc151* is specifically expressed in the ventral node, marked with an asterisk in panel I showing a view from the left. Panel II shows a ventral view. Abbreviations are as follows: A, anterior; P, posterior.

(B) Sequence of the *Ccdc151*$^{Snbl}$ homozygous mutant mouse (RefSeq NM_029939) compared to a wild-type littermate shows a c.828+2A>G substitution affecting the exon 6 splice donor site, with the exon-intron boundary shown by a dashed red line and intronic sequence distinguished from exonic sequence by lower case.

(C) Transmission electron microscopy of tracheal cilia from wild-type and a *Ccdc151*$^{Snbl}$ homozygous mutant mouse reveals the lack of outer dynein arms in the mutant (blue arrowheads). Scale bars represent 0.1 μm.

*(legend continued on next page)*

were static (Movies S1 and S2). In the pronephric tubules, ciliary motility appeared less affected because cilia were able to bundle and beat regularly; however, the mutant cilia beat with significantly reduced beat frequency compared to those in unaffected sibling embryos (Figures 2G and S2; Movies S3 and S4). TEM ultrastructural analysis of pronephric cilia from *flanders* mutants revealed a loss of the ciliary outer dynein arms (Figure 2H).

### A Putative *ccdc151* Ortholog Is Required for Proper Cilia Function in Planarians

Interestingly, a putative *ccdc151* ortholog (amino acid similarity 56%; identity 33%) is also required for proper cilia function in planarians (Figure S4). Planarians are flatworms that move on a ventral ciliated epithelium (Figures S4A–S4A′) and defects in cilia function cause characteristic locomotion defects.[57] Hence, planarian locomotion represents a simple readout for cilia dysfunction. We found that *ccdc151* RNAi-treated planarians (Figure S4C) had severely reduced locomotive ability, moving only by contracting their muscles rather than gliding (Figures S4D–S4D′; Movies S5 and S6). TEM analysis revealed a loss of ODAs in the mutant axonemes compared to control axonemes, consistent with the findings in zebrafish and mouse *CCDC151* mutants (Figure S4E). Together, these data support an evolutionarily conserved role for *ccdc151* in establishing proper ciliary motility in vertebrates and invertebrates.

### *Ccdc151* Is Expressed at the Mouse Embryonic Node and *Ccdc151*-Deficient Mice Exhibit Immotile and Dyskinetic Cilia and Laterality Defects

To further examine the developmental aspects of *Ccdc151* function, we performed WISH on mouse embryos examined at embryonic day E7.5 when the node is present. This identified specific expression of *Ccdc151* in the ventral node, consistent with the zebrafish analysis (Figure 3A). To examine the consequence of *Ccdc151* deficiency on embryonic development, we further investigated the mouse model using a mutant, *Snowball* (*Snbl*), which was recovered from a large-scale mouse mutagenesis screen for mutations causing congenital heart defects.[58] Whole mouse exome sequencing analysis in *Snowball* homozygous mutants identified five homozygous coding variants (Table S5) that were genotyped across all the mutants from the same family. However, a single-base substitution in the highly conserved +2 canonical splice donor site of *Ccdc151* (RefSeq NM_029939.3) exon 6, c.828+2A>G (Figure 3B), was the only candidate mutation that was homozygous in all the mutants, thus indicating it is disease causing (Table S5). This substitution causes anomalous splicing, as shown by RT-PCR using tracheal RNA isolated from wild-type and homozygous *Snowball* mutants and primers spanning the gene, which all yielded no RT-PCR products in *Ccdc151*$^{Snbl}$ mutants compared to controls (Figure S5). The *Ccdc151*$^{Snbl}$ allele therefore appears to convey a loss-of-function mutation subject to nonsense-mediated decay similar to that of zebrafish *flanders* mutants. Analysis of the tracheal airway epithelia by high-speed videomicroscopy showed largely immotile cilia in *Ccdc151*$^{Snbl}$ mutants as compared to the normal rapid synchronous beating of the wild-type littermates (Movie S7). Similarly, the ependymal cilia lining the brain ventricles of mutants were largely immotile, with occasional patches exhibiting very slow and stiff ciliary motion, while rapid synchronous ciliary motion was observed in the ependymal tissue of wild-type littermates (Movie S8). TEM of tracheal cilia from homozygous mutant *Ccdc151*$^{Snbl}$ mice showed a specific loss of the ciliary outer dynein arms (Figure 3C). We also performed high-resolution IF microscopy of *Snowball* tracheal epithelia using antibodies to mouse axonemal dynein heavy chain DNAH5, which is a subunit of the ODA complexes, present in both the distal and proximal ODA types present in respiratory cilia.[59] This showed that DNAH5 is undetectable in *Ccdc151*$^{Snbl}$ cilia, consistent with a defect of ODA assembly in the ciliary axonemes (Figure 3D).

Phenotyping analysis of homozygous *Ccdc151*$^{Snbl}$ mutant animals showed a spectrum of features with three distinct laterality phenotypes, as detailed in Table S6. Mutants displayed either situs solitus with normal visceral organ situs (Figure 3E, panel I), situs inversus totalis with mirror-image symmetric organ situs (Figure 3E, panel II), or heterotaxy with discordant or randomized organ situs (Figure 3E, panel III). In the latter case of more complex heterotaxy, a typical mutant exhibited normal heart orientation (levocardia) and lung lobation, but inverted liver lobation with dextrogastria (Figure 3E, panel III). Among mutants surviving to term, 33% exhibited heterotaxy

(D) Air-dried tracheal airway epithelia from wild-type and *Ccdc151*$^{Snbl}$ mutant mice costained for acetylated α-tubulin (green) and the ODA component DNAH5 (red) were visualized by immunofluorescence microscopy. Nuclei were stained with DAPI (blue). In control mice, DNAH5 localized to the axonemes stained with acetylated α-tubulin (top panels), but in *Ccdc151*$^{Snbl}$ mutant airway epithelia, DNAH5 is undetectable in the ciliary axonemes (bottom panels) Scale bars represent 10 μm.
(E) Homozygous *Ccdc151*$^{Snbl}$ mutants exhibit a spectrum of laterality defects including situs solitus (I), situs inversus totalis (II), or heterotaxy (III). In I–III, heart situs is denoted by arrows, lung lobation is numbered 1–5 (white numbers), and liver lobation is numbered 1–3 (black numbers); Stm indicates stomach. Dextrocardia, inverted lung lobation, inverted liver lobation, and dextrogastria are seen in the situs inversus totalis mutant (II) as compared to the normal visceral organ situs observed in the situs solitus mutant (I). A mutant with heterotaxy (III) exhibits levocardia with normal heart orientation and lung lobation but inverted liver lobation and dextrogastria. Analysis of the cardiovascular anatomy of two *Ccdc151*$^{Snbl}$ mutants with heterotaxy revealed one with congenital heart defects (V) comprising dextrocardia with duplicated inferior vena cava (IVC) and a ventricular septal defect (VSD; VIII) and another mutant heart with a coronary artery fistula spanning from the left coronary artery to the left ventricle (VI, IX). For comparison, the heart from a normal control animal with situs solitus is shown (IV, VII). The R-L double arrow in (I) indicates right-left orientation, which is the same for all panels. Abbreviations: LV, left ventricle; RV, right ventricle.

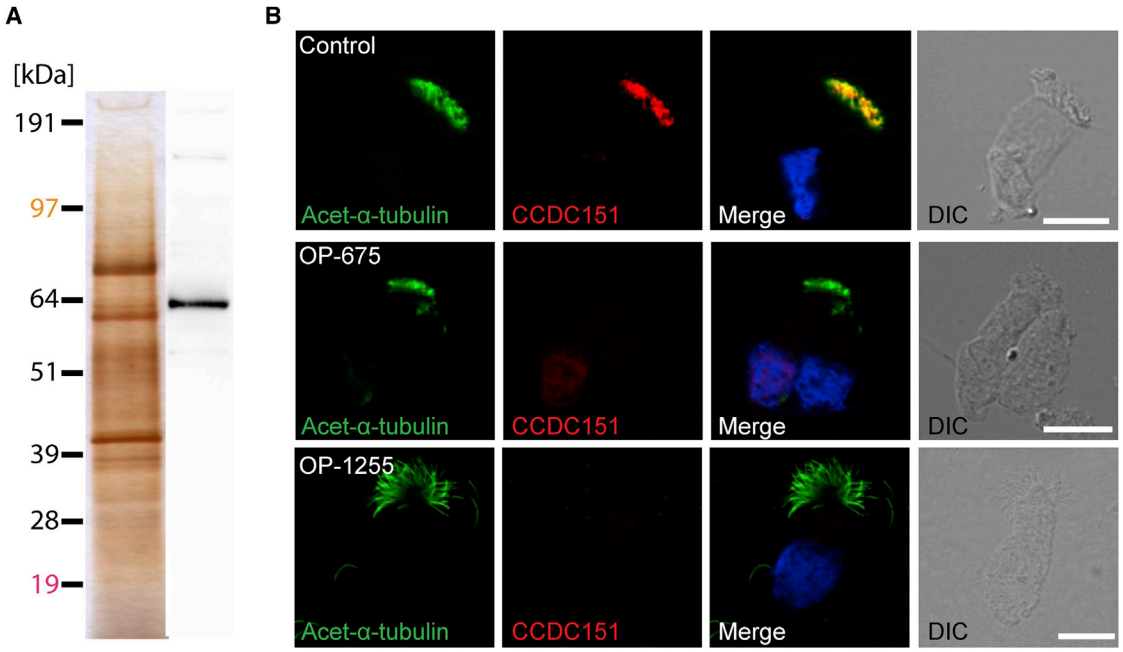


**Figure 4. CCDC151 Is Localized to Respiratory Ciliary Axonemes**
(A) Immunoblot analysis (right lane) of protein lysates (left lane) from human respiratory cells compared to protein standard show that CCDC151 antibodies specifically detect a single protein band corresponding to the predicted size (~64 kDa).
(B) Respiratory epithelial cells obtained by nasal biopsy of unaffected individuals and PCD-affected individuals carrying *CCDC151* mutations were double labeled with antibodies directed against acetylated α-tubulin (green) and CCDC151 (red). Nuclei were stained with Hoechst 33342 (blue). Both proteins colocalize (yellow) along the ciliary axonemes in cells from the healthy controls, while in respiratory cells of OP-675 and OP-1255 carrying *CCDC151* recessive loss-of-function mutations, CCDC151 is not detectable in the ciliary axonemes. Scale bars represent 10 μm.

and 66% had either situs inversus or situs solitus. These findings are consistent with observations from other mouse models of PCD such as *Dnah5*, *Armc4*, and *Dyx1c1* mutants.[21,27,48] Consistent with other PCD mouse models, congenital heart defects observed in *Ccdc151*$^{Snbl}$ mutants included dextrocardia with a duplicated inferior vena cava (Figure 3E, panel V). This was confirmed by histopathology examination of intracardiac anatomy with 3D reconstruction using episcopic confocal microscopy, which also revealed a muscular ventricular septal defect (VSD) akin to that seen in the affected individual OP-675 carrying *CCDC151* mutations (Figure 3E, panel VIII). In another heterotaxic mutant, a coronary fistula was detected by videomicroscopy of the contracting heart (Figure 3E, panel VI and Movie S9) and confirmed by episcopic confocal microscopy 3D reconstruction (Figure 3E, panel IX). As documented in detail in Table S6, in addition to abdominal inversion and abnormal lung lobation and bronchial branching, other heart defects were noted including inverted outflow tract. Together, these findings confirm *Snowball* to be an informative PCD mouse model.

### CCDC151 Localizes to Respiratory Ciliary Axonemes and *CCDC151* Mutations Are Associated with Loss of the Ciliary Outer Dynein Arms and Ciliary Immotility in Humans

To further explore the role of CCDC151 in human disease, we next examined protein localization in respiratory ciliated cells. We first screened protein lysates isolated from human nasal respiratory epithelial cells using commercially available rabbit polyclonal antibodies directed against CCDC151. Immunoblot analysis showed that the antibodies specifically recognize CCDC151, detecting a single protein band of the predicted molecular weight (~64 kDa) (Figure 4A). We then used this antibody to analyze the subcellular localization of the protein in human motile respiratory cilia. IF showed that CCDC151 localizes to the axonemes of wild-type human respiratory epithelial cells, overlapping with an acetylated α-tubulin marker of ciliary axonemes. However, the protein was undetectable in the respiratory cilia of individuals OP-675 and OP-1255, consistent with the predicted loss-of-function consequences of the *CCDC151* nonsense mutations they carry (Figure 4B). We used high-speed videomicroscopy to analyze respiratory ciliary beating in individuals with *CCDC151* mutations. Both individuals OP-675 and OP-1255 had completely immotile cilia compared to the coordinated synchronous beating of cilia from unaffected control individuals, recapitulating the functional defects of the *Ccdc151*$^{Snbl}$ mice (Movies S10, S11, and S12).

Ultrastructural analysis by TEM of respiratory ciliary axonemes from individuals carrying *CCDC151* mutations showed a loss of the outer dynein arms (mean of ODAs detected: 0.8–0.9) from ciliary axonemes compared to those of unaffected control individuals (ODA mean: 7.5–9) (Figure 5C). These results are consistent with the

ultrastructural ciliary phenotype of *ccdc151*$^{ts272a}$ (*flanders*) mutants, *ccdc151* RNAi planarians, and *Ccdc151*$^{Snbl}$ mice (Figures 2H, S4E, and 3C). We further examined this defect at the molecular level by immunofluorescence staining of the respiratory cells of individuals OP-675 and OP-1255 using antibodies directed against two established markers of human dynein arm integrity, the ODA marker DNAH5 and IDA marker DNALI1 (which is a light intermediate dynein associated with some IDAs). DNAH5 was undetectable in the axonemes of *CCDC151* mutant individuals, suggesting that CCDC151 deficiency likely causes a disruption of axonemal ODA assembly (Figure 5A). In contrast, DNALI1 correctly localized to the axonemes of both individuals' respiratory cells. This marker showed a similar distribution to that of control individual's cilia (Figure 5B), suggesting that *CCDC151* mutations do not alter assembly of IDA proteins.

Together, the TEM and IF data indicate that the axonemes of CCDC151-deficient cilia have ODA defects but that DNALI1-related IDA assembly is undisturbed. We also examined the integrity of the ciliary nexin dynein regulatory complexes (N-DRC) in *CCDC151* mutant cilia by immunolocalization using antibodies directed against an integral N-DRC component, GAS8 (human DRC4).[33–35] Similarly to DNALI1, GAS8 correctly localized to mutant ciliary axonemes, indicating that N-DRC assembly is not affected (Figure 5B).

### CCDC151 Plays a Role in Assembly of the Outer Dynein Arm Docking Complex in Addition to Its Role in Outer Dynein Arm Assembly

To further understand the functional role of CCDC151 in ODA assembly, we also studied the localization of CCDC114, which is an ODA-DC subunit responsible for axonemal microtubule attachment of the ODAs[16] in *CCDC151* mutant cilia. We found that CCDC114 was undetectable in the respiratory cilia of *CCDC151*-mutant individuals compared to the normal axonemal localization of CCDC114 in respiratory cilia from unaffected controls (Figure 6A). This suggests that the axonemal localization of CCDC114 is CCDC151 dependent. Since the localization of the ODA-DC-related ARMC4 is known to be CCDC114 dependent,[21] we also studied ARMC4 localization in *CCDC151* mutant cilia. ARMC4 was also undetectable in the respiratory cilia of *CCDC151* mutant individuals, indicating that similarly to CCDC114, the axonemal localization of ARMC4 is CCDC151 dependent (Figure 6B).

Considering the similarities in phenotype caused by *CCDC114* and *CCDC151* mutations with regard to ODA defects,[16] we tested for possible interactions between these proteins. Using myc- and FLAG-tagged proteins that were coexpressed in HEK293 cells, we found by coimmunoprecipitation that CCDC151 interacted with CCDC114 (Figure 6C), but not DNAI1, DNAI2, and DNAL1, whose mutations also cause ODA defects (data not shown). We confirmed the reciprocal interaction between CCDC114 and CCDC151 by yeast two-hybrid analysis (Figure S6).

## Discussion

In this study, we describe loss-of-function nonsense mutations in *CCDC151* in five individuals with PCD from three unrelated families. CCDC151 is a coiled-coil-domain-containing protein conserved in motile ciliated species, and the *Chlamydomonas* ortholog ODA10 has recently been described as critical for axonemal motility.[53] CCDC151 was also recently shown to be critical for motility of intraflagellar (IFT)-dependent cilia in *Drosophila* and expressed in motile cilia of zebrafish.[54] The identified human *CCDC151* mutations are predicted to result in the failure to produce a functional CCDC151, and this was verified by immunofluorescence studies on nasal respiratory epithelial cilia of affected individuals.

In humans, we find that *CCDC151* deficiency causes PCD with randomization of left-right body asymmetry. This is consistent with evidence from zebrafish showing that ablation of *ccdc151* in *flanders* mutants as well as morpholino-induced *ccdc151* depletion leads to a randomization of left-right body asymmetry, as reported here and in a prior study.[54] Similarly, we find that homozygous mutant *Ccdc151*$^{Snbl}$ mice display laterality defects ranging from situs inversus to a spectrum of situs anomalies associated with heterotaxy. Also consistent with these data is the finding that the zebrafish and mouse orthologs of *CCDC151* are expressed in left-right organizers during embryonic development. The *Ccdc151*$^{Snbl}$ mutants with heterotaxy manifested with congenital heart defects, displaying intracardiac anomalies including inverted outflow tract, ventricular septal defects, and dual inferior vena cava. A variable displacement of other visceral organs (liver, gut, abdomen) was also observed, as well as abnormal lung lobation and bronchial branching. This mirrors the laterality phenotypes recorded in all but one of the five individuals carrying *CCDC151* mutations that are reported here.

In *CCDC151* mutant human cilia, we found that the ODA component DNAH5 is not detectable in the ciliary axonemes, indicating that CCDC151 deficiency leads to defects of both known ODA types present in the proximal and distal ciliary axonemes.[59] This is confirmed by the absence of ODAs in ultrastructurally analyzed cross-sections from *CCDC151* mutant cilia, corresponding to the ciliary immotility observed by high-speed video microscopy. In agreement with these data, *CCDC151*-deficient *Chlamydomonas*, fly, zebrafish (*flanders* and morphants), planarians, and *Ccdc151*$^{Snbl}$ mice all have defective ciliary motility associated with a lack of axonemal ODAs.[53,54] In contrast, we found that the axonemal IDA component DNALI1 was normal in *CCDC151* mutant cilia, suggesting that CCDC151 deficiency does not result in defects of IDA axonemal assembly.

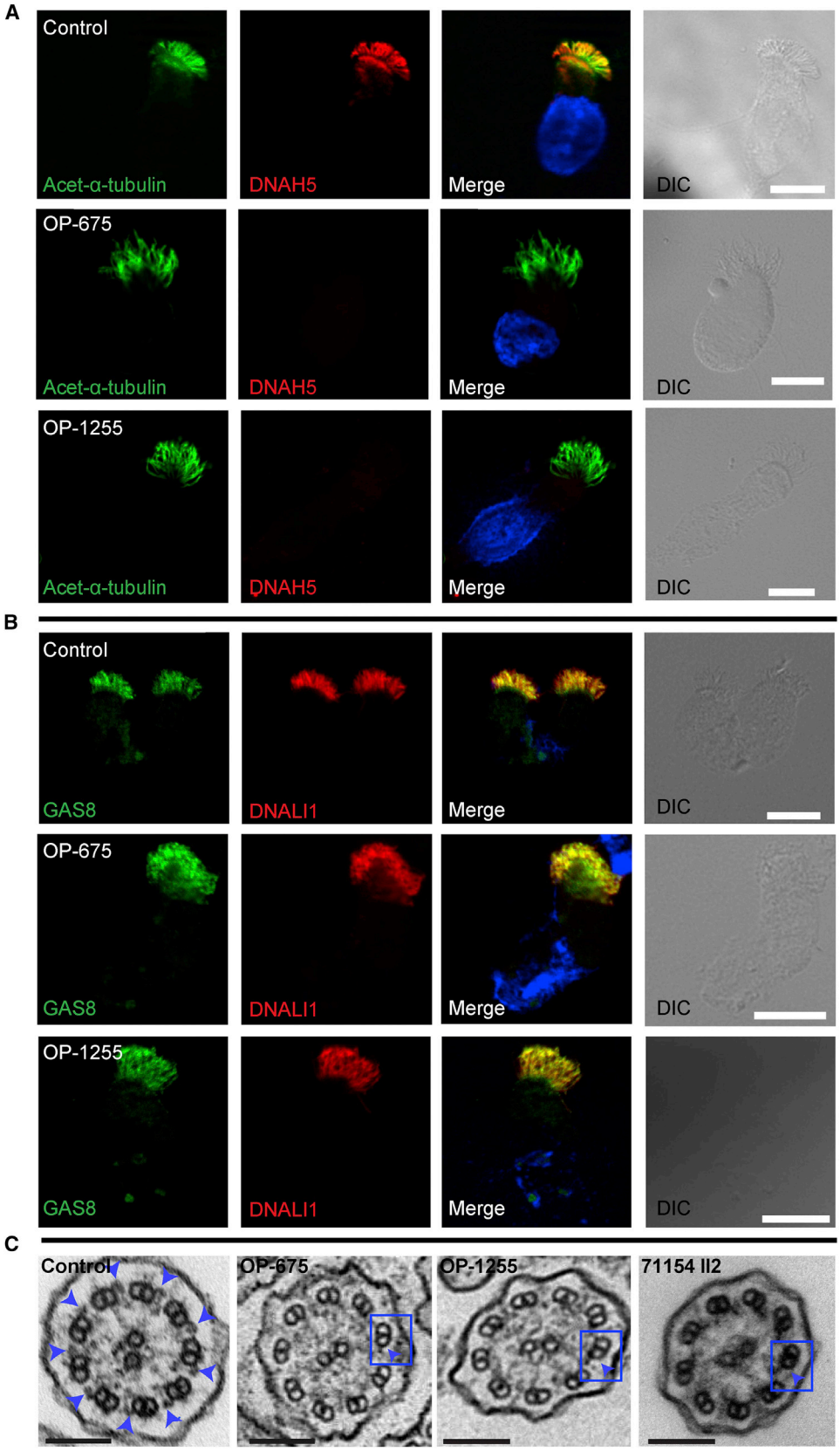


**Figure 5. *CCDC151* Mutations Result in Defects of the Outer Dynein Arms**
(A) Respiratory epithelial cells from control and PCD-affected individuals OP-675 and OP-1255 carrying *CCDC151* mutations were double-labeled with antibodies directed against acetylated α-tubulin (green) and DNAH5 (red). Both proteins colocalize (yellow) along the cilia in cells from the unaffected control. In contrast, in *CCDC151* mutant, DNAH5 is not detectable in the ciliary axonemes.

*(legend continued on next page)*

Using an antibody that specifically detects the native CCDC151 in human respiratory epithelial cells, we found a predominantly axonemal localization of CCDC151. These results contrast with previous reports from studies in *Chlamydomonas* and *Drosophila* chordotonal neuron cilia that showed dual localization for CCDC151 orthologs in both the cilia/flagella and cytosolic compartments.[53,54] These reported studies were based on overexpression of epitope-tagged forms of CCDC151, and it is possible that human cilia do contain cytosol-localized CCDC151 but at levels below our IF detection ability. Mutations causing PCD have been found in a number of cytosolic and cytosolic/axonemal dual localized factors, at least some of which are known to be involved in the preassembly of the ciliary dynein motors within the cell body prior to their import into cilia (SPAG1, DNAAF1, DNAAF2, HEATR2, DNAAF3, DYX1C1, ZMYND10, LRRC6, C21orf59, and CCDC103).[22–32] However, causal mutations in this class of protein have so far all been associated with combined ODA and IDA deficiency, which is distinct from the isolated ODA deficiency arising from *CCDC151* mutations. Therefore, despite axonemal and cytoplasmic colocalization for CCDC151 suggested from model systems, CCDC151 is not likely to function as a "typical" cytoplasmic dynein arm assembly factor.

Here, we found that CCDC114 and ARMC4 are undetectable in the ciliary axonemes of *CCDC151* mutant individuals, indicating that their ciliary localization is CCDC151 dependent. Moreover, we demonstrate that CCDC151 and CCDC114 interact together by coimmunoprecipitation analyses. Fundamental to the process of assembly and attachment of the dynein arms into axonemes is the correct targeting and docking of the ODAs via the ODA docking complex (ODA-DC) system, and human CCDC114 and ARMC4 have been implicated as integral or associated ODA-DC proteins, representing essential components for attachment of ODAs into ciliary axonemes. Furthermore, mutations in *ARMC4* and *CCDC114* cause PCD with outer dynein arm defects similarly to the *CCDC151* mutations reported here.[15,16,21,60,61] CCDC114 is the vertebrate ortholog of the *Chlamydomonas* ODA-DC component DC2.[15,16] *Chlamydomonas* has two other ODA-DC proteins, the coiled-coil DC1 and the EF-hand DC3/DLE3,[62,63] which still have no defined vertebrate orthologs. The armadillo-repeat ARMC4 has been shown to be CCDC114 dependent for its localization into axonemes and to be involved in the correct targeting and docking of the ODAs.[21] These data therefore suggest that CCDC151 is required for assembly of ODAs as well as ODA-DCs into axonemes.

Recent work showing that the *Chlamydomonas* ortholog of CCDC151, ODA10, is not an integral ODA component but is required for ODA assembly[53] add to growing evidence for the existence of an accessory complex to the ODA-DC in *Chlamydomonas* that is independent from the ODA-DC. This ODA-DC accessory complex is thought to be composed of three subunits: ODA10 in addition to ODA5 and ODA8.[64–66] It can thus be considered unlikely that human CCDC151 is a structural component of the ODAs or the ODA-DCs themselves. Rather, the loss of CCDC114 and ARMC4 from *CCDC151*-mutated cilia and the direct interaction between CCDC151 and CCDC114 point to a role for CCDC151 in the assembly or other activities of the ODA docking complex. *Chlamydomonas* studies have shown that ODA10/CCDC151 might have a role in converting the ODAs into a form with higher binding affinity for their axonemal binding sites, and hence acting at a key step in the final association of dynein complexes with their docking sites.[53]

Multisubunit axonemal dynein arm complexes contain heavy, intermediate, and light chain dyneins, and dyneins form a diverse protein family with roles in many different types of cellular movement, such as vesicle transport, nuclear migration, chromosome movements, spindle formation and orientation, and beating of cilia and flagella.[67] The correct attachment of specific dyneins to different cell structures plays a major role in the maintenance of many essential cell functions.[68] Therefore, dissecting out the mechanisms by which dyneins are targeted to and bind to cell organelles are of substantial interest. Current evidence suggests that CCDC151 is an atypical PCD-associated protein, probably not an integral component of the ODA-docking complex but required for correct axonemal docking and targeting of ODAs and essential for the assembly of both the ODAs and the ODA-DC apparatus.

Discovery of additional causal mutations underlying PCD has clinical significance for improving genetic and clinical diagnosis of this condition and facilitating improved counselling of affected families. In one consanguineous family (71154), we identified mutations after first narrowing down the regions of interest for gene identification by mapping autozygous regions of interest. Here, using whole-exome sequencing output to provide a combined mapping/sequencing use of NGS data proves a powerful approach for discovery of PCD-causing mutations, which often affects consanguineous families.[69] *CCDC151* mutations appear to be a rare cause of PCD since next-generation sequencing of collectively more than 280 affected individuals by the London and Leeds group has

(B) Respiratory epithelial cells from control and PCD-affected individuals OP-675 and OP-1255 carrying *CCDC151* mutations were double-labeled with antibodies directed against the N-DRC component GAS8 (green) and DNALI1 (red). Both proteins colocalize (yellow) along the cilia in cells from the unaffected control as well as both of the PCD-affected individuals. Scale bars represent 10 μm.
(C) Transmission electron micrographs of cross-sections through respiratory epithelial cell cilia show an absence of the outer dynein arms in PCD-affected individuals with *CCDC151* mutations (right panels, blue box and arrow), compared to a control individual without PCD. In the healthy control, outer dynein arms (left panel, blue arrows) are visible. Scale bars represent 0.1 μm.

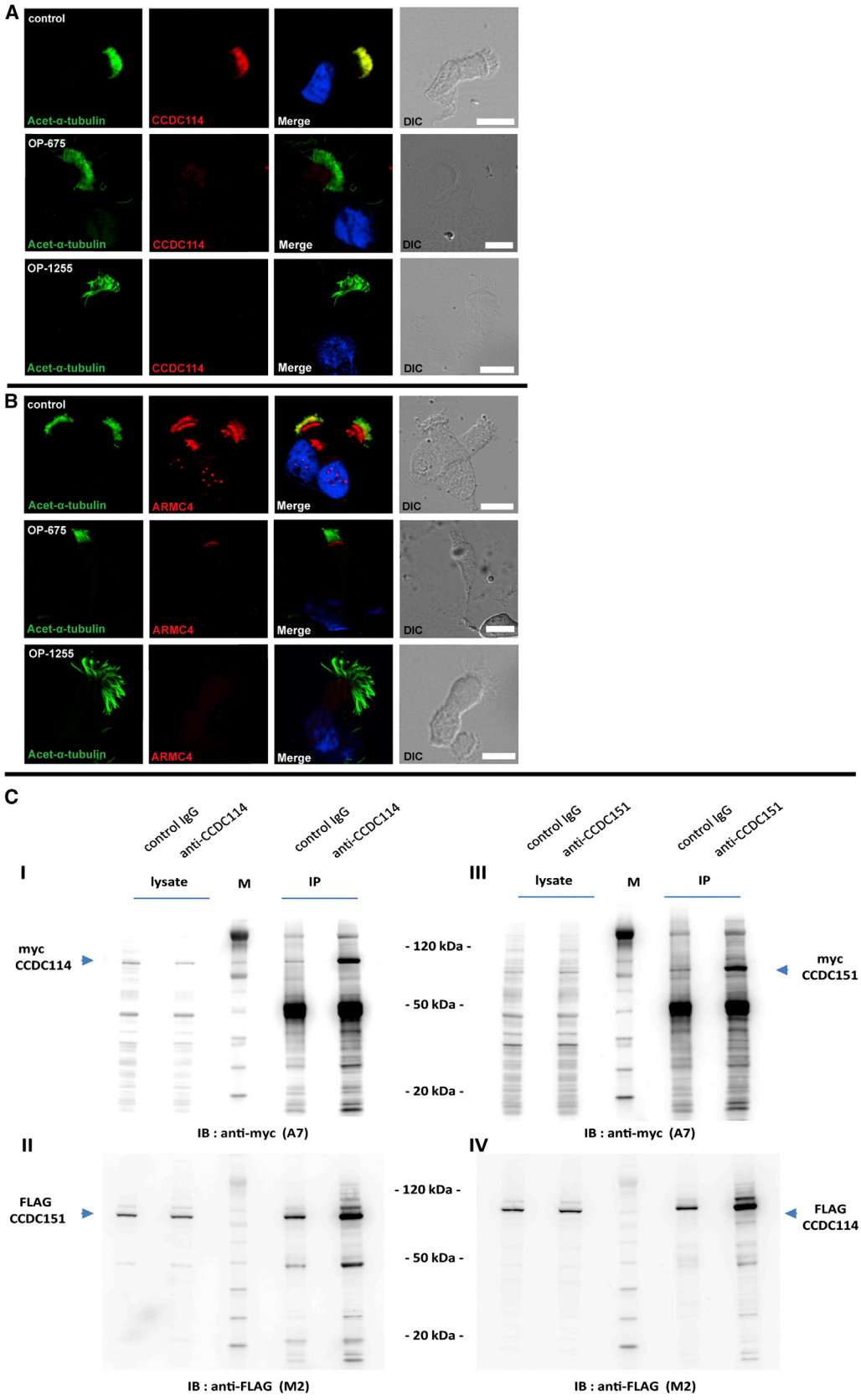


**Figure 6. Mutations in *CCDC151* Affect the Localization of ODA-Microtubule Docking-Complex-Associated Components CCDC114 and ARMC4 in Human Respiratory Cells and the ODA-Associated CCDC151 Interacts with CCDC114**

(A and B) Respiratory epithelial cells from an unaffected control and PCD-affected individuals carrying *CCDC151* mutations were double-labeled with antibodies directed against acetylated α-tubulin (green) and CCDC114 (A, red) or ARMC4 (B, red). CCDC114 and

*(legend continued on next page)*

detected only two affected families, and only one further affected family was detected out of 150 displaying ODA defects that were screened in Germany. The c.925G>T nonsense variant was detected in two unrelated pedigrees of Arabic origin. We cannot rule out a founder mutation, because we were not able to compare haplotypes. ODA assembly and docking are complex molecular mechanisms that should be studied in more depth in order to identify therapeutic approaches for treatment of individuals affected with PCD. Thus the identification of mutations in *CCDC151* provides an important step forward in understanding the complex biology of ODA assembly in motile cilia and flagella.

## Supplemental Data

Supplemental Data include 6 figures, 6 tables, and 12 movies and can be found with this article online at http://dx.doi.org/10.1016/j.ajhg.2014.08.005.

## Acknowledgments

We thank the PCD individuals and their families, the German patient support group "Kartagener Syndrom und Primaere Ciliaere Dyskinesie e.V.," and the UK PCD Family Support Group. We thank Badie Jacob for clinical diagnostic studies. We thank M. Herting, L. Overkamp, F.J. Seesing, P. Fischer, and M. Patel for technical work, M. Turmaine for TEM, and Maria Philipsen for assistance. We are grateful to the UK10K consortium (investigators listed at http://www.uk10k.org/), in particular the Rare Diseases Group, for making this study possible. This work was supported by NICHD grant 2R01HD048584 to C.E.S. and R.D.B., NHLBI grant U01-HL098180 to C.W.L., NRW Research School "Cell Dynamics and Disease, CEDAD" to R.H. and H.O., "Deutsche Forschungsgemeinschaft" (DFG OM 6/4), the IZKF (Om2/009/12) Muenster, Schröder Stiftung, and Kindness for Kids to H.O., SYSCILIA (EU FP7 GA nr. 241955) to H.O. and R.R., NWO (Vici-016.130.664) to R.R., BESTCILIA (EU FP7 GA nr. 305404) to H.O. and K.G.N., the Max Planck Society and the DFG (SFB629) to K.B., "Studies of nucleic acids and proteins - from basic to applied research" within the International PhD Projects Programme of Foundation for Polish Science, cofinanced by European Union - Regional Development Fund, for M.K., Wellcome Trust award WT091310 to UK10K, Great Ormond Street Hospital Children's Charity to H.M.M., Milena Carvajal Pro-Kartagener Foundation, Action Medical Research (GN2101), and Newlife Foundation for Disabled Children UK (10-11/15) to H.M.M. and E.M.K.C., and MRC grant MR/L01629X/1 to C.M.W., I.M.C., C.P.D., and E.S. Open Access publication charges for this article were funded by the Wellcome Trust.

Received: May 23, 2014
Accepted: August 14, 2014
Published: September 4, 2014

## Web Resources

The URLs for data presented herein are as follows:

1000 Genomes, http://browser.1000genomes.org
AgileExomeFilter, http://dna.leeds.ac.uk/agile/AgileExomeFilter/
AgileMultiIdeogram, http://dna.leeds.ac.uk/agile/AgileMultiIdeogram/
ANNOVAR, http://www.openbioinformatics.org/annovar/
dbSNP, http://www.ncbi.nlm.nih.gov/projects/SNP/
GATK, http://www.broadinstitute.org/gatk/
GenBank, http://www.ncbi.nlm.nih.gov/genbank/
NHLBI Exome Sequencing Project (ESP) Exome Variant Server, http://evs.gs.washington.edu/EVS/
Online Mendelian Inheritance in Man (OMIM), http://www.omim.org/
SMART, http://www.smart.embl-heidelberg.de/
UK10K Consortium, http://www.uk10k.org/

## Accession Numbers

The GenBank accession number for *Smed-ccdc151* reported in this paper is KM281511.

## References

1. Fliegauf, M., Benzing, T., and Omran, H. (2007). When cilia go bad: cilia defects and ciliopathies. Nat. Rev. Mol. Cell Biol. *8*, 880–893.
2. Yoshiba, S., and Hamada, H. (2014). Roles of cilia, fluid flow, and Ca2+ signaling in breaking of left-right symmetry. Trends Genet. *30*, 10–17.
3. Brokaw, C.J. (1994). Control of flagellar bending: a new agenda based on dynein diversity. Cell Motil. Cytoskeleton *28*, 199–204.
4. Sharma, N., Berbari, N.F., and Yoder, B.K. (2008). Ciliary dysfunction in developmental abnormalities and diseases. Curr. Top. Dev. Biol. *85*, 371–427.
5. Zariwala, M.A., Knowles, M.R., and Omran, H. (2007). Genetic defects in ciliary structure and function. Annu. Rev. Physiol. *69*, 423–450.
6. Kennedy, M.P., Omran, H., Leigh, M.W., Dell, S., Morgan, L., Molina, P.L., Robinson, B.V., Minnix, S.L., Olbrich, H., Severin, T., et al. (2007). Congenital heart disease and other heterotaxic defects in a large cohort of patients with primary ciliary dyskinesia. Circulation *115*, 2814–2821.

ARMC4 colocalize with acetylated α-tubulin along control ciliary axonemes (merge, yellow). However, in respiratory cells from individuals OP-675 and OP-1255 carrying mutations in *CCDC151*, CCDC114 and ARMC4 are undetectable in the ciliary axonemes. Scale bars represent 10 μm.
(C) HEK293 lysates coexpressing FLAG or myc epitope-tagged CCDC151 and CCDC114 were immunoprecipitated with either rabbit control IgG and rabbit anti-CCDC151 or anti-CCDC114 antibody. Immunoblotting with mouse anti-myc or anti-FLAG antibody demonstrates that CCDC114 immunoprecipitates CCDC151 (I, II) and CCDC151 immunoprecipitates CCDC114 (III, IV). The open reading frames of recombinant CCDC151 and CCDC114 are 595 and 670 amino acids, respectively. The observed approximate molecular weights of 85 and 100 kDa, respectively, represent additional sequence from myc- and FLAG epitope tags. Equal volumes (12 μl) of lysate and immunoprecipitate fractions were loaded on the same gel; lysate fractions represent 0.5% of total lysate (1 ml volume) and immunoprecipitate fractions represent 1/15 lysis volume (33 μl resuspension). Magic Mark protein ladder (M) was used to estimate molecular weight of recombinant CCDC151 and CCDC114.

7. Shapiro, A.J., Davis, S.D., Ferkol, T., Dell, S.D., Rosenfeld, M., Olivier, K.N., Sagel, S.D., Milla, C., Zariwala, M.A., Wolf, W., et al.; for the Genetic Disorders of Mucociliary Clearance Consortium (2014). Laterality defects other than situs inversus totalis in primary ciliary dyskinesia: insights into situs ambiguus and heterotaxy. Chest *13*, 1704.
8. Wallmeier, J., Al-Mutairi, D.A., Chen, C.T., Loges, N.T., Pennekamp, P., Menchen, T., Ma, L., Shamseldin, H.E., Olbrich, H., Dougherty, G.W., et al. (2014). Mutations in CCNO result in congenital mucociliary clearance disorder with reduced generation of multiple motile cilia. Nat. Genet. *46*, 646–651.
9. Shoemark, A., Dixon, M., Corrin, B., and Dewar, A. (2012). Twenty-year review of quantitative transmission electron microscopy for the diagnosis of primary ciliary dyskinesia. J. Clin. Pathol. *65*, 267–271.
10. Papon, J.F., Coste, A., Roudot-Thoraval, F., Boucherat, M., Roger, G., Tamalet, A., Vojtek, A.M., Amselem, S., and Escudier, E. (2010). A 20-year experience of electron microscopy in the diagnosis of primary ciliary dyskinesia. Eur. Respir. J. *35*, 1057–1063.
11. Onoufriadis, A., Shoemark, A., Schmidts, M., Patel, M., Jimenez, G., Liu, H., Thomas, B., Dixon, M., Hirst, R.A., Rutman, A., et al.; UK10K (2014). Targeted NGS gene panel identifies mutations in RSPH1 causing primary ciliary dyskinesia and a common mechanism for ciliary central pair agenesis due to radial spoke defects. Hum. Mol. Genet. *23*, 3362–3374.
12. Zariwala, M.A., Omran, H., and Ferkol, T.W. (2011). The emerging genetics of primary ciliary dyskinesia. Proc. Am. Thorac. Soc. *8*, 430–433.
13. Olbrich, H., Häffner, K., Kispert, A., Völkel, A., Volz, A., Sasmaz, G., Reinhardt, R., Hennig, S., Lehrach, H., Konietzko, N., et al. (2002). Mutations in DNAH5 cause primary ciliary dyskinesia and randomization of left-right asymmetry. Nat. Genet. *30*, 143–144.
14. Bartoloni, L., Blouin, J.L., Pan, Y., Gehrig, C., Maiti, A.K., Scamuffa, N., Rossier, C., Jorissen, M., Armengot, M., Meeks, M., et al. (2002). Mutations in the DNAH11 (axonemal heavy chain dynein type 11) gene cause one form of situs inversus totalis and most likely primary ciliary dyskinesia. Proc. Natl. Acad. Sci. USA *99*, 10282–10286.
15. Knowles, M.R., Leigh, M.W., Ostrowski, L.E., Huang, L., Carson, J.L., Hazucha, M.J., Yin, W., Berg, J.S., Davis, S.D., Dell, S.D., et al.; Genetic Disorders of Mucociliary Clearance Consortium (2013). Exome sequencing identifies mutations in *CCDC114* as a cause of primary ciliary dyskinesia. Am. J. Hum. Genet. *92*, 99–106.
16. Onoufriadis, A., Paff, T., Antony, D., Shoemark, A., Micha, D., Kuyt, B., Schmidts, M., Petridi, S., Dankert-Roelse, J.E., Haarman, E.G., et al.; UK10K (2013). Splice-site mutations in the axonemal outer dynein arm docking complex gene CCDC114 cause primary ciliary dyskinesia. Am. J. Hum. Genet. *92*, 88–98.
17. Mazor, M., Alkrinawi, S., Chalifa-Caspi, V., Manor, E., Sheffield, V.C., Aviram, M., and Parvari, R. (2011). Primary ciliary dyskinesia caused by homozygous mutation in DNAL1, encoding dynein light chain 1. Am. J. Hum. Genet. *88*, 599–607.
18. Pennarun, G., Escudier, E., Chapelin, C., Bridoux, A.M., Cacheux, V., Roger, G., Clément, A., Goossens, M., Amselem, S., and Duriez, B. (1999). Loss-of-function mutations in a human gene related to *Chlamydomonas reinhardtii* dynein IC78 result in primary ciliary dyskinesia. Am. J. Hum. Genet. *65*, 1508–1519.
19. Loges, N.T., Olbrich, H., Fenske, L., Mussaffi, H., Horvath, J., Fliegauf, M., Kuhl, H., Baktai, G., Peterffy, E., Chodhari, R., et al. (2008). DNAI2 mutations cause primary ciliary dyskinesia with defects in the outer dynein arm. Am. J. Hum. Genet. *83*, 547–558.
20. Duriez, B., Duquesnoy, P., Escudier, E., Bridoux, A.M., Escalier, D., Rayet, I., Marcos, E., Vojtek, A.M., Bercher, J.F., and Amselem, S. (2007). A common variant in combination with a nonsense mutation in a member of the thioredoxin family causes primary ciliary dyskinesia. Proc. Natl. Acad. Sci. USA *104*, 3336–3341.
21. Hjeij, R., Lindstrand, A., Francis, R., Zariwala, M.A., Liu, X., Li, Y., Damerla, R., Dougherty, G.W., Abouhamed, M., Olbrich, H., et al. (2013). ARMC4 mutations cause primary ciliary dyskinesia with randomization of left/right body asymmetry. Am. J. Hum. Genet. *93*, 357–367.
22. Knowles, M.R., Ostrowski, L.E., Loges, N.T., Hurd, T., Leigh, M.W., Huang, L., Wolf, W.E., Carson, J.L., Hazucha, M.J., Yin, W., et al. (2013). Mutations in SPAG1 cause primary ciliary dyskinesia associated with defective outer and inner dynein arms. Am. J. Hum. Genet. *93*, 711–720.
23. Loges, N.T., Olbrich, H., Becker-Heck, A., Häffner, K., Heer, A., Reinhard, C., Schmidts, M., Kispert, A., Zariwala, M.A., Leigh, M.W., et al. (2009). Deletions and point mutations of LRRC50 cause primary ciliary dyskinesia due to dynein arm defects. Am. J. Hum. Genet. *85*, 883–889.
24. Omran, H., Kobayashi, D., Olbrich, H., Tsukahara, T., Loges, N.T., Hagiwara, H., Zhang, Q., Leblond, G., O'Toole, E., Hara, C., et al. (2008). Ktu/PF13 is required for cytoplasmic pre-assembly of axonemal dyneins. Nature *456*, 611–616.
25. Horani, A., Druley, T.E., Zariwala, M.A., Patel, A.C., Levinson, B.T., Van Arendonk, L.G., Thornton, K.C., Giacalone, J.C., Albee, A.J., Wilson, K.S., et al. (2012). Whole-exome capture and sequencing identifies *HEATR2* mutation as a cause of primary ciliary dyskinesia. Am. J. Hum. Genet. *91*, 685–693.
26. Mitchison, H.M., Schmidts, M., Loges, N.T., Freshour, J., Dritsoula, A., Hirst, R.A., O'Callaghan, C., Blau, H., Al Dabbagh, M., Olbrich, H., et al. (2012). Mutations in axonemal dynein assembly factor DNAAF3 cause primary ciliary dyskinesia. Nat. Genet. *44*, 381–389, S1–S2.
27. Tarkar, A., Loges, N.T., Slagle, C.E., Francis, R., Dougherty, G.W., Tamayo, J.V., Shook, B., Cantino, M., Schwartz, D., Jahnke, C., et al.; UK10K (2013). DYX1C1 is required for axonemal dynein assembly and ciliary motility. Nat. Genet. *45*, 995–1003.
28. Zariwala, M.A., Gee, H.Y., Kurkowiak, M., Al-Mutairi, D.A., Leigh, M.W., Hurd, T.W., Hjeij, R., Dell, S.D., Chaki, M., Dougherty, G.W., et al. (2013). ZMYND10 is mutated in primary ciliary dyskinesia and interacts with LRRC6. Am. J. Hum. Genet. *93*, 336–345.
29. Moore, D.J., Onoufriadis, A., Shoemark, A., Simpson, M.A., zur Lage, P.I., de Castro, S.C., Bartoloni, L., Gallone, G., Petridi, S., Woollard, W.J., et al. (2013). Mutations in ZMYND10, a gene essential for proper axonemal assembly of inner and outer dynein arms in humans and flies, cause primary ciliary dyskinesia. Am. J. Hum. Genet. *93*, 346–356.
30. Kott, E., Duquesnoy, P., Copin, B., Legendre, M., Dastot-Le Moal, F., Montantin, G., Jeanson, L., Tamalet, A., Papon, J.F., Siffroi, J.P., et al. (2012). Loss-of-function mutations in LRRC6, a gene essential for proper axonemal assembly of inner and outer dynein arms, cause primary ciliary dyskinesia. Am. J. Hum. Genet. *91*, 958–964.

31. Austin-Tse, C., Halbritter, J., Zariwala, M.A., Gilberti, R.M., Gee, H.Y., Hellman, N., Pathak, N., Liu, Y., Panizzi, J.R., Patel-King, R.S., et al. (2013). Zebrafish ciliopathy screen plus human mutational analysis identifies C21orf59 and CCDC65 defects as causing primary ciliary dyskinesia. Am. J. Hum. Genet. *93*, 672–686.
32. Panizzi, J.R., Becker-Heck, A., Castleman, V.H., Al-Mutairi, D.A., Liu, Y., Loges, N.T., Pathak, N., Austin-Tse, C., Sheridan, E., Schmidts, M., et al. (2012). CCDC103 mutations cause primary ciliary dyskinesia by disrupting assembly of ciliary dynein arms. Nat. Genet. *44*, 714–719.
33. Merveille, A.C., Davis, E.E., Becker-Heck, A., Legendre, M., Amirav, I., Bataille, G., Belmont, J., Beydon, N., Billen, F., Clément, A., et al. (2011). CCDC39 is required for assembly of inner dynein arms and the dynein regulatory complex and for normal ciliary motility in humans and dogs. Nat. Genet. *43*, 72–78.
34. Becker-Heck, A., Zohn, I.E., Okabe, N., Pollock, A., Lenhart, K.B., Sullivan-Brown, J., McSheene, J., Loges, N.T., Olbrich, H., Haeffner, K., et al. (2011). The coiled-coil domain containing protein CCDC40 is essential for motile cilia function and left-right axis formation. Nat. Genet. *43*, 79–84.
35. Wirschell, M., Olbrich, H., Werner, C., Tritschler, D., Bower, R., Sale, W.S., Loges, N.T., Pennekamp, P., Lindberg, S., Stenram, U., et al. (2013). The nexin-dynein regulatory complex subunit DRC1 is essential for motile cilia function in algae and humans. Nat. Genet. *45*, 262–268.
36. Castleman, V.H., Romio, L., Chodhari, R., Hirst, R.A., de Castro, S.C., Parker, K.A., Ybot-Gonzalez, P., Emes, R.D., Wilson, S.W., Wallis, C., et al. (2009). Mutations in radial spoke head protein genes RSPH9 and RSPH4A cause primary ciliary dyskinesia with central-microtubular-pair abnormalities. Am. J. Hum. Genet. *84*, 197–209.
37. Olbrich, H., Schmidts, M., Werner, C., Onoufriadis, A., Loges, N.T., Raidt, J., Banki, N.F., Shoemark, A., Burgoyne, T., Al Turki, S., et al.; UK10K Consortium (2012). Recessive HYDIN mutations cause primary ciliary dyskinesia without randomization of left-right body asymmetry. Am. J. Hum. Genet. *91*, 672–684.
38. Bukowy-Bieryłło, Z., Ziętkiewicz, E., Loges, N.T., Wittmer, M., Geremek, M., Olbrich, H., Fliegauf, M., Voelkel, K., Rutkiewicz, E., Rutland, J., et al. (2013). RPGR mutations might cause reduced orientation of respiratory cilia. Pediatr. Pulmonol. *48*, 352–363.
39. Ferrante, M.I., Zullo, A., Barra, A., Bimonte, S., Messaddeq, N., Studer, M., Dollé, P., and Franco, B. (2006). Oral-facial-digital type I protein is required for primary cilia formation and left-right axis specification. Nat. Genet. *38*, 112–117.
40. Knowles, M.R., Daniels, L.A., Davis, S.D., Zariwala, M.A., and Leigh, M.W. (2013). Primary ciliary dyskinesia. Recent advances in diagnostics, genetics, and characterization of clinical disease. Am. J. Respir. Crit. Care Med. *188*, 913–922.
41. Barbato, A., Frischer, T., Kuehni, C.E., Snijders, D., Azevedo, I., Baktai, G., Bartoloni, L., Eber, E., Escribano, A., Haarman, E., et al. (2009). Primary ciliary dyskinesia: a consensus statement on diagnostic and treatment approaches in children. Eur. Respir. J. *34*, 1264–1276.
42. Watson, C.M., Crinnion, L.A., Morgan, J.E., Harrison, S.M., Diggle, C.P., Adlard, J., Lindsay, H.A., Camm, N., Charlton, R., Sheridan, E., et al. (2014). Robust diagnostic genetic testing using solution capture enrichment and a novel variant-filtering interface. Hum. Mutat. *35*, 434–441.
43. Carr, I.M., Bhaskar, S., O'Sullivan, J., Aldahmesh, M.A., Shamseldin, H.E., Markham, A.F., Bonthron, D.T., Black, G., and Alkuraya, F.S. (2013). Autozygosity mapping with exome sequence data. Hum. Mutat. *34*, 50–56.
44. Jaffe, K.M., Thiberge, S.Y., Bisher, M.E., and Burdine, R.D. (2010). Imaging cilia in zebrafish. Methods Cell Biol. *97*, 415–435.
45. Sullivan-Brown, J., Bisher, M.E., and Burdine, R.D. (2011). Embedding, serial sectioning and staining of zebrafish embryos using JB-4 resin. Nat. Protoc. *6*, 46–55.
46. Schottenfeld, J., Sullivan-Brown, J., and Burdine, R.D. (2007). Zebrafish curly up encodes a Pkd2 ortholog that restricts left-side-specific expression of southpaw. Development *134*, 1605–1615.
47. Shen, Y., Leatherbury, L., Rosenthal, J., Yu, Q., Pappas, M.A., Wessels, A., Lucas, J., Siegfried, B., Chatterjee, B., Svenson, K., and Lo, C.W. (2005). Cardiovascular phenotyping of fetal mice by noninvasive high-frequency ultrasound facilitates recovery of ENU-induced mutations causing congenital cardiac and extracardiac defects. Physiol. Genomics *24*, 23–36.
48. Tan, S.Y., Rosenthal, J., Zhao, X.Q., Francis, R.J., Chatterjee, B., Sabol, S.L., Linask, K.L., Bracero, L., Connelly, P.S., Daniels, M.P., et al. (2007). Heterotaxy and complex structural heart defects in a mutant mouse model of primary ciliary dyskinesia. J. Clin. Invest. *117*, 3742–3752.
49. Francis, R., and Lo, C.W. (2013). Ex vivo method for high resolution imaging of cilia motility in rodent airway epithelia. J. Vis. Exp. http://dx.doi.org/10.3791/50343.
50. Hom, E.F., Witman, G.B., Harris, E.H., Dutcher, S.K., Kamiya, R., Mitchell, D.R., Pazour, G.J., Porter, M.E., Sale, W.S., Wirschell, M., et al. (2011). A unified taxonomy for ciliary dyneins. Cytoskeleton (Hoboken) *68*, 555–565.
51. Alsaadi, M.M., Gaunt, T.R., Boustred, C.R., Guthrie, P.A., Liu, X., Lenzi, L., Rainbow, L., Hall, N., Alharbi, K.K., and Day, I.N. (2012). From a single whole exome read to notions of clinical screening: primary ciliary dyskinesia and RSPH9 p.Lys268del in the Arabian Peninsula. Ann. Hum. Genet. *76*, 211–220.
52. Alkuraya, F.S. (2013). The application of next-generation sequencing in the autozygosity mapping of human recessive diseases. Hum. Genet. *132*, 1197–1211.
53. Dean, A.B., and Mitchell, D.R. (2013). *Chlamydomonas* ODA10 is a conserved axonemal protein that plays a unique role in outer dynein arm assembly. Mol. Biol. Cell *24*, 3689–3696.
54. Jerber, J., Baas, D., Soulavie, F., Chhin, B., Cortier, E., Vesque, C., Thomas, J., and Durand, B. (2014). The coiled-coil domain containing protein CCDC151 is required for the function of IFT-dependent motile cilia in animals. Hum. Mol. Genet. *23*, 563–577.
55. Mason, J.M., and Arndt, K.M. (2004). Coiled coil domains: stability, specificity, and biological implications. ChemBioChem *5*, 170–176.
56. Haffter, P., Granato, M., Brand, M., Mullins, M.C., Hammerschmidt, M., Kane, D.A., Odenthal, J., van Eeden, F.J., Jiang, Y.J., Heisenberg, C.P., et al. (1996). The identification of genes with unique and essential functions in the development of the zebrafish, *Danio rerio*. Development *123*, 1–36.
57. Rompolas, P., Patel-King, R.S., and King, S.M. (2010). An outer arm Dynein conformational switch is required for metachronal synchrony of motile cilia in planaria. Mol. Biol. Cell *21*, 3669–3679.
58. Liu, X.Q., Francis, R., Kim, A.J., Ramirez, R., Chen, G., Subramanian, R., Anderton, S., Kim, Y., Wong, L., Morgan,

J., et al. (2014). Interrogating congenital heart defects with noninvasive fetal echocardiography in a mouse forward genetic screen. Circ Cardiovasc Imaging *7*, 31–42.
59. Fliegauf, M., Olbrich, H., Horvath, J., Wildhaber, J.H., Zariwala, M.A., Kennedy, M., Knowles, M.R., and Omran, H. (2005). Mislocalization of DNAH5 and DNAH9 in respiratory cells from patients with primary ciliary dyskinesia. Am. J. Respir. Crit. Care Med. *171*, 1343–1349.
60. Onoufriadis, A., Shoemark, A., Munye, M.M., James, C.T., Schmidts, M., Patel, M., Rosser, E.M., Bacchelli, C., Beales, P.L., Scambler, P.J., et al.; UK10K (2014). Combined exome and whole-genome sequencing identifies mutations in ARMC4 as a cause of primary ciliary dyskinesia with defects in the outer dynein arm. J. Med. Genet. *51*, 61–67.
61. Wu, D.H., and Singaraja, R.R. (2013). Loss-of-function mutations in CCDC114 cause primary ciliary dyskinesia. Clin. Genet. *83*, 526–527.
62. Takada, S., Wilkerson, C.G., Wakabayashi, K., Kamiya, R., and Witman, G.B. (2002). The outer dynein arm-docking complex: composition and characterization of a subunit (oda1) necessary for outer arm assembly. Mol. Biol. Cell *13*, 1015–1029.
63. Casey, D.M., Inaba, K., Pazour, G.J., Takada, S., Wakabayashi, K., Wilkerson, C.G., Kamiya, R., and Witman, G.B. (2003). DC3, the 21-kDa subunit of the outer dynein arm-docking complex (ODA-DC), is a novel EF-hand protein important for assembly of both the outer arm and the ODA-DC. Mol. Biol. Cell *14*, 3650–3663.
64. Kamiya, R. (1988). Mutations at twelve independent loci result in absence of outer dynein arms in *Chylamydomonas reinhardtii*. J. Cell Biol. *107*, 2253–2258.
65. Fowkes, M.E., and Mitchell, D.R. (1998). The role of preassembled cytoplasmic complexes in assembly of flagellar dynein subunits. Mol. Biol. Cell *9*, 2337–2347.
66. Wirschell, M., Pazour, G., Yoda, A., Hirono, M., Kamiya, R., and Witman, G.B. (2004). Oda5p, a novel axonemal protein required for assembly of the outer dynein arm and an associated adenylate kinase. Mol. Biol. Cell *15*, 2729–2741.
67. Holzbaur, E.L., and Vallee, R.B. (1994). DYNEINS: molecular structure and cellular function. Annu. Rev. Cell Biol. *10*, 339–372.
68. Vallee, R.B., and Sheetz, M.P. (1996). Targeting of motor proteins. Science *271*, 1539–1544.
69. Lucas, J.S., Burgess, A., Mitchison, H.M., Moya, E., Williamson, M., and Hogg, C.; on behalf of the National PCD service, UK (2014). Diagnosis and management of primary ciliary dyskinesia. Arch. Dis. Child. Published online April 25, 2014. http://dx.doi.org/10.1136/archdischild-2013-304831.

**The American Journal of Human Genetics, Volume *95***

**Supplemental Data**

# *CCDC151* Mutations Cause Primary Ciliary Dyskinesia by Disruption of the Outer Dynein Arm Docking Complex Formation

**Rim Hjeij, Alexandros Onoufriadis, Christopher M. Watson, Christopher E. Slagle, Nikolai T. Klena, Gerard W. Dougherty, Małgorzata Kurkowiak, Niki T. Loges, Christine P. Diggle, Nicholas F.C. Morante, George C. Gabriel, Kristi L. Lemke, You Li, Petra Pennekamp, Tabea Menchen, Franziska Konert, June Kehlet Martin, Dorus A. Mans, Stef J.F. Letteboer, Claudius Werner, Thomas Burgoyne, Cordula Westermann, Andrew Rutman, Ian M. Carr, Christopher O'Callaghan, Eduardo Moya, Eddie M.K. Chung, UK10K, Eamonn Sheridan, Kim G. Nielsen, Ronald Roepman, Kerstin Bartscherer, Rebecca D. Burdine, Cecilia W. Lo, Heymut Omran, and Hannah M. Mitchison**

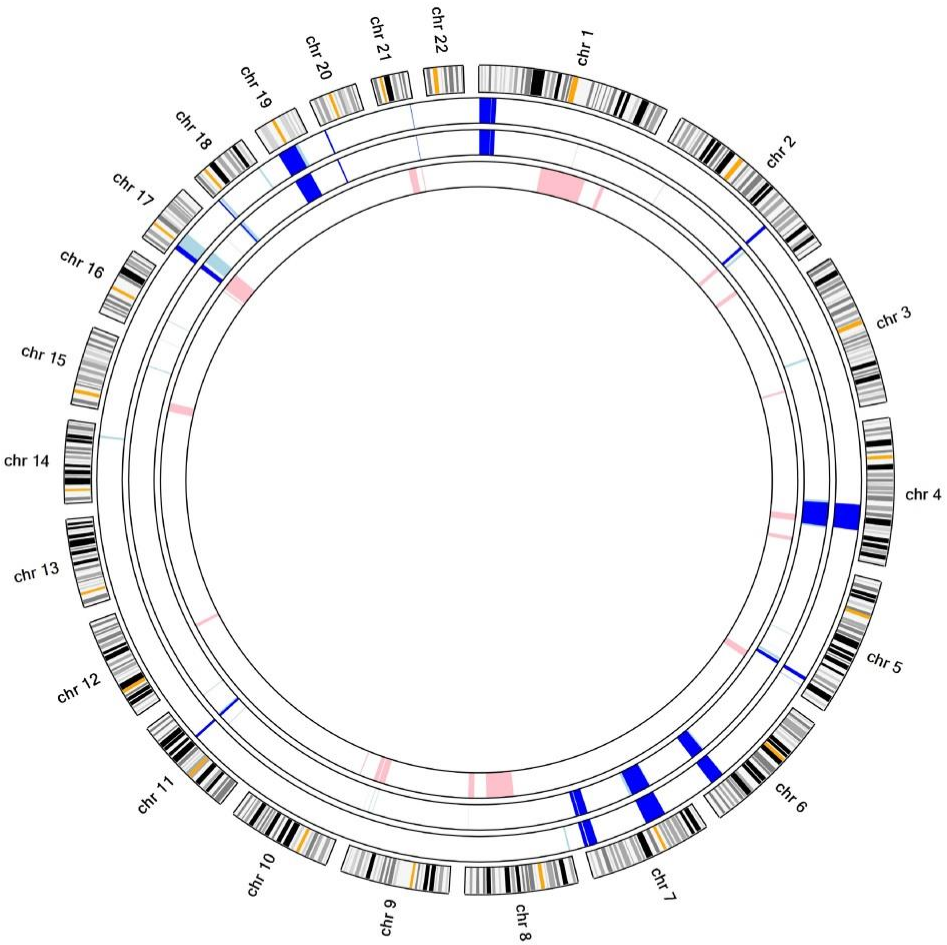


| Chromosome | Start | End | Interval size (bp) |
|---|---|---|---|
| 1 | 554,484 | 16,731,510 | 16,177,026 |
| 1 | 17,295,679 | 23,885,498 | 6,589,819 |
| 2 | 175,624,107 | 180,047,908 | 4,423,801 |
| 4 | 114,120,520 | 149,993,092 | 35,872,572 |
| 5 | 155,935,708 | 160,914,508 | 4,978,800 |
| 6 | 132,508,426 | 152,540,278 | 20,031,852 |
| 7 | 38,119,969 | 67,702,531 | 29,582,562 |
| 7 | 140,159,721 | 152,350,013 | 12,190,292 |
| 7 | 153,696,994 | 158,811,981 | 5,114,987 |
| 11 | 83,296,734 | 86,955,572 | 3,658,838 |
| 17 | 14,005,439 | 21,147,404 | 7,141,965 |
| 18 | 2,305,761 | 4,460,922 | 2,155,161 |
| 19 | 9,297,273 | 35,843,086 | 26,545,813 |
| 20 | 1,669,250 | 3,870,124 | 2,200,874 |
| 21 | 43,504,228 | 43,969,714 | 465,486 |

**Figure S1. Autozygosity mapping in family 71154**. A MultiIdeogram graphical plot of SNP (Affymetrix Genome-Wide Human SNP Array v6.0) versus exome data shows an autozygosity mapping output indicating regions of homozygosity on each chromosome. The image shows the chromosomes alongside SNP array data for the affected sibling 71154 II:2 (outer circle), exome data from the affected sibling (middle circle) and SNP array data from the unaffected sibling 71154 II:1 (inner circle). Regions of homozygosity are shown in light blue for the affected and pink for the unaffected. Dark blue shows homozygous regions shared across both data types in the affected, that are not present in the unaffected sibling, including a large region on chr19 spanning the *CCDC151* gene. Co-ordinates of the 15 dark blue autozygous regions identified as present in the affected but not unaffected sibling are shown in **Table S2**.

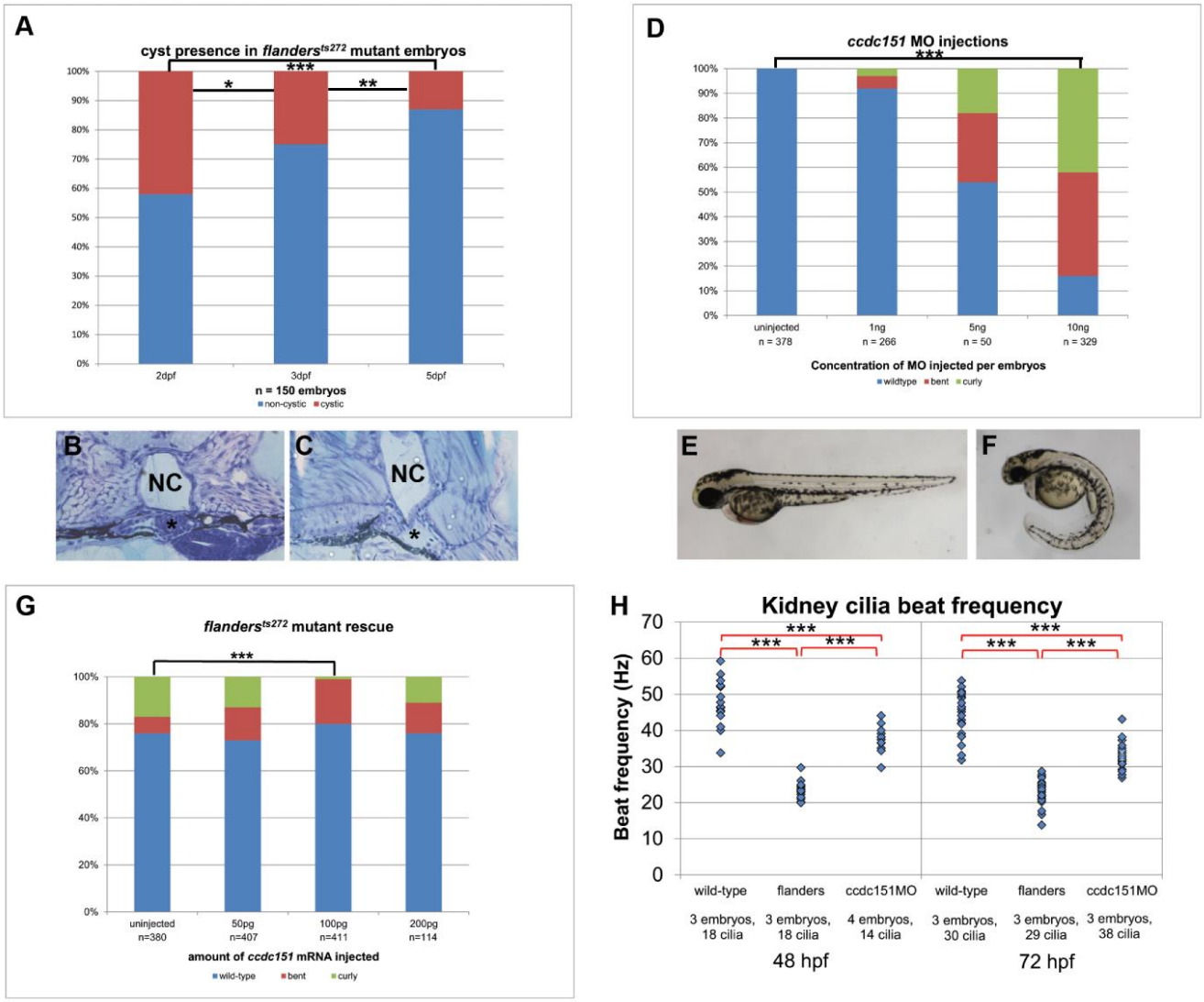


**Figure S2. Additional characterization of *flanders*$^{ts272}$ mutants and *ccdc151* morpholino injected embryos.** (**A**) Frequency of pronephric cysts in *flanders* mutants. 150 mutant embryos, identified by the tail curl phenotype, were scored on three consecutive days for the presence of pronephric cysts. Pronephric cysts were qualitatively smaller than those we observe in mutants that more severely disrupt cilia motility. Cyst presence diminished over time suggesting that the cysts could resolve in the mutant embryos. chi-squared p-value * 0.002 between day 1 and 2, ** 0.005 between day 2 and 3, and *** $<10^{-8}$ between day 1 and 3. (**B**) Cross section of a wildtype sibling and (**C**) a *flanders* mutant kidney cyst. The glomerulus (asterisk) lies underneath the notochord (NC) and is dilated in mutant embryos. (**D**) Injection of a splice-blocking *ccdc151* morpholino can phenocopy the tail curl observed in *flanders* mutants producing tight curled tails (**F**) or tails with a slightly less pronounced curl (bent; not shown). Compare these phenotypes to those observed in **E** (uninjected). These phenotypes are dose dependent. *** chi-squared p-value $<10^{-114}$ (**G**) The tail curl observed in *flanders*$^{ts272}$ mutant embryos can be partially rescued by injection of 100pg of *ccdc151* RNA per embryo. Higher and lower concentrations were not as effective at rescuing the tail curl phenotype. RNA was injected into clutches of embryos from *flanders*$^{ts272/+}$ heterozygote parents. Thus 25% of the embryos are expected to be *flanders*$^{ts272}$ mutants. *** chi-squared p-value $<10^{-16}$ (**H**) Quantification of pronephric cilia beat frequency in *flanders* mutants, *ccdc151* morpholino (MO) injected and siblings at 48hpf and 72hpf. *** student's t-test p-value $< 10^{-16}$ . Data from Figure 2 is reproduced here for comparison. The morpholino injected embryos displayed slightly higher beat frequencies compared to *flanders* mutants, yet morpholino injected embryos still had reduced frequencies compared to wild-type embryos.

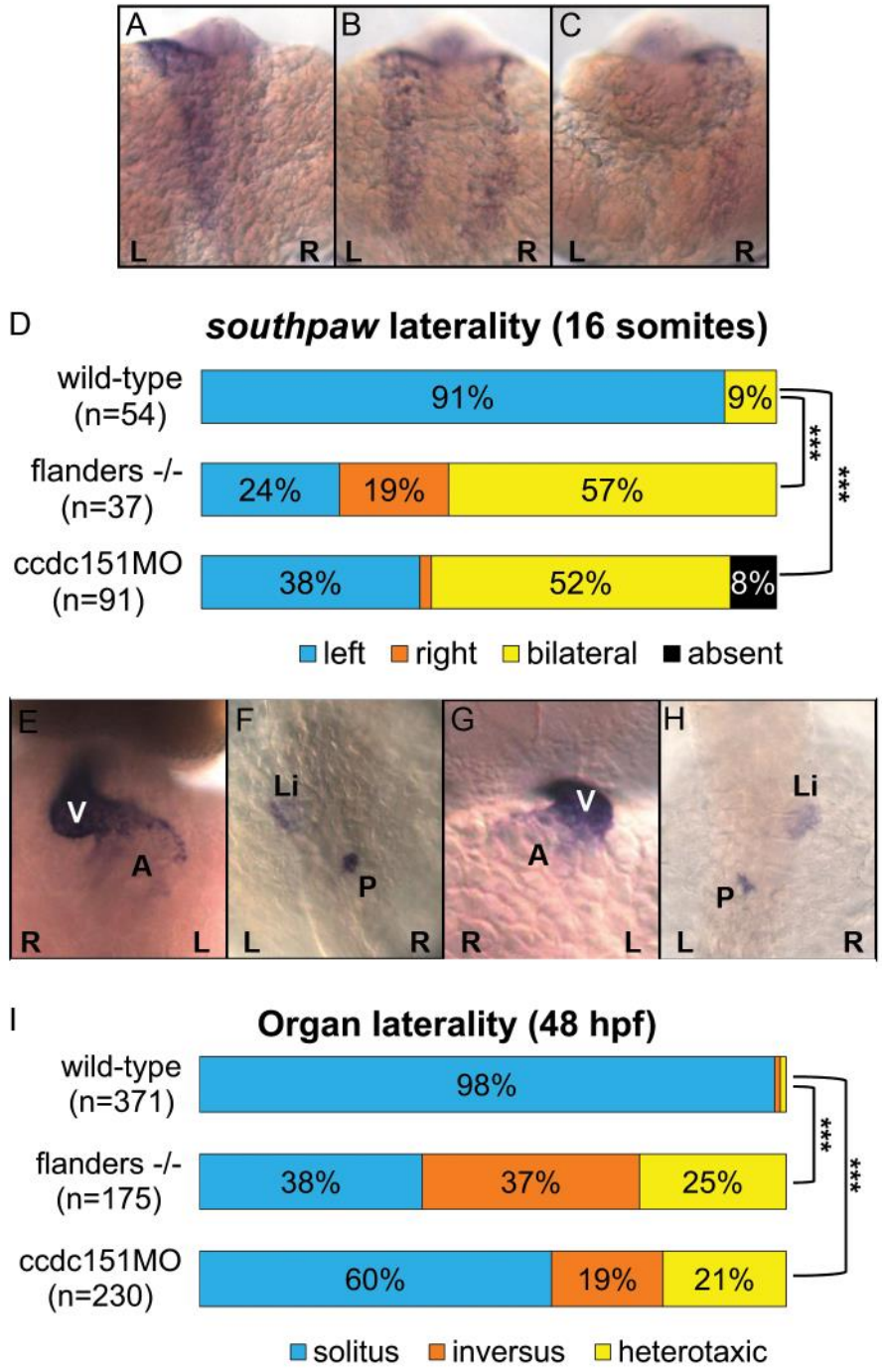


**Figure S3. Left-right patterning defects observed in *flanders*$^{ts272}$ mutants and *ccdc151* morpholino injected embryos.** Representative embryos expressing *southpaw* by *in situ* hybridization on the (**A**) left, (**B**) both sides, or (**C**) right within the lateral plate mesoderm of 16 somite embryos. (**D**) Quantification of *southpaw* expression patterns in wild-type versus *flanders* mutants and *ccdc151* morpholino injected embryos. Data from Figure 2 is reproduced here for comparison. *** chi squared p-value < $10^{-9}$ (**E-H**) *in situ* hybridization to visualize the heart (*myl7*), pancreas (*insulin*) and liver (*fkd2*) as described[48]. In wild-type embryos the heart (E; ventral view) loops to the right placing the ventricle (V) to the right of the atrium (**A**). (F; dorsal view) the liver (Li) is on the left and the pancreas (P) is on the right. In *flanders* mutants and *ccdc151* morpholino injected embryos, the heart and viscera can be reversed (*situs inversus*) as shown in the embryo pictured in (**G**) and (**H**), or heterotaxic referring to a randomized positioning of these organs with respect to one another. (**I**) Quantification of organ laterality in wild-type versus *flanders* mutants and *ccdc151* morpholino injected embryos. Data from Figure 2 is reproduced here for comparison. *** chi-squared p-value < $10^{-55}$. Left (L) and right (R) are indicated.

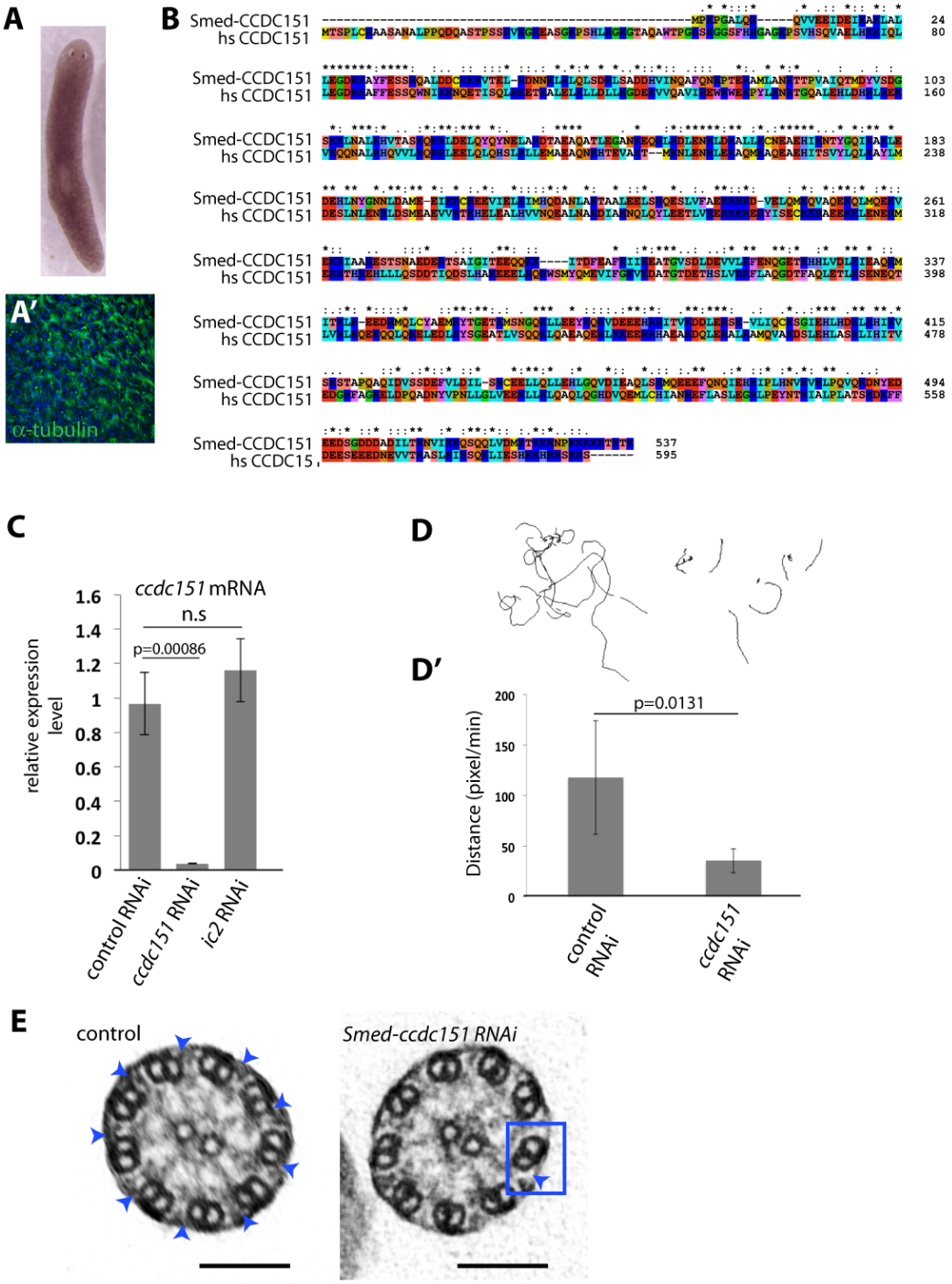


**Figure S4. A putative *ccdc151* ortholog (*Smed-ccdc151*) is required for cilia-mediated locomotion in the planarian species *Schmidtea mediterranea*.** (**A**) Planarians (adult *Schmidtea mediterranea*) in (A)) move on ventral cilia, which can be visualized with an antibody against acetylated alpha-tubulin (A'). (**B**) Alignment of *Smed*-CCDC151 with human CCDC151 using ClustalX (http://www.clustal.org). Amino acids with similar properties are color-coded by similar colors. Planarian flatworms of the species *Schmidtea mediterranea* (Clonal Line BCN-10) were kept in the dark in plastic tanks filled with artificial water at 19°C. The water was changed twice a week and planarians were fed once a week with calf liver. Animals were starved 7 days prior RNAi experiments. RNAi was performed as previously described[46]. dsRNAs against green fluorescent protein mRNA (*gfp*) and *Smed-ic2* mRNA[47] were used as controls. The locomotion phenotype observed after *Smed-ccdc151* RNAi was confirmed with two independent dsRNAs. Primer sequences are listed below. To extract total RNA we used TRIzol reagent (Invitrogen) and cDNA was synthesized using RevertAid First Strand cDNA Synthesis Kit (Thermo Scientific). Quantitative PCR reactions were performed

using the TaqMan Universal PCR Master Mix (Applied Biosystems) and knockdown efficiency was determined using the Real-Time PCR System 7500 (Applied Biosystems). Three biological replicates were measured in duplicates. *Gapdh* was used as reference gene. Primer sequences are listed below. (**C**) Quantitative real-time PCR analysis of *Smed-ccdc151* mRNA expression levels after *gfp* (control), *Smed-ic2*, or *Smed-ccdc151* RNAi. *Smed-ccdc151* expression levels are strongly reduced after *ccdc151* RNAi but not after RNAi of the control genes *gfp* or *Smed-ic2*. Error bars represent standard deviations of the mean of three biological replicates. (**D, D'**) Locomotion assay with *gfp* and *Smed-ccdc151* RNAi animals quantifying traveled distance (D') where 3x 10 animals were scored, and representative paths travelled by 10 animals (D). We used the Intas iX UV-Gel-Imager to take sequential Pictures (1 picture per second for 1 min) of RNAi animals. The animals were placed in the center of a container covered with a minimal volume of water with their dorsal side up. Images were analyzed with Fiji. (**E**) TEM analysis shows a loss of outer dynein arms in *Smed-ccdc151* RNAi compared to controls. Scales bars, 0.1µm.

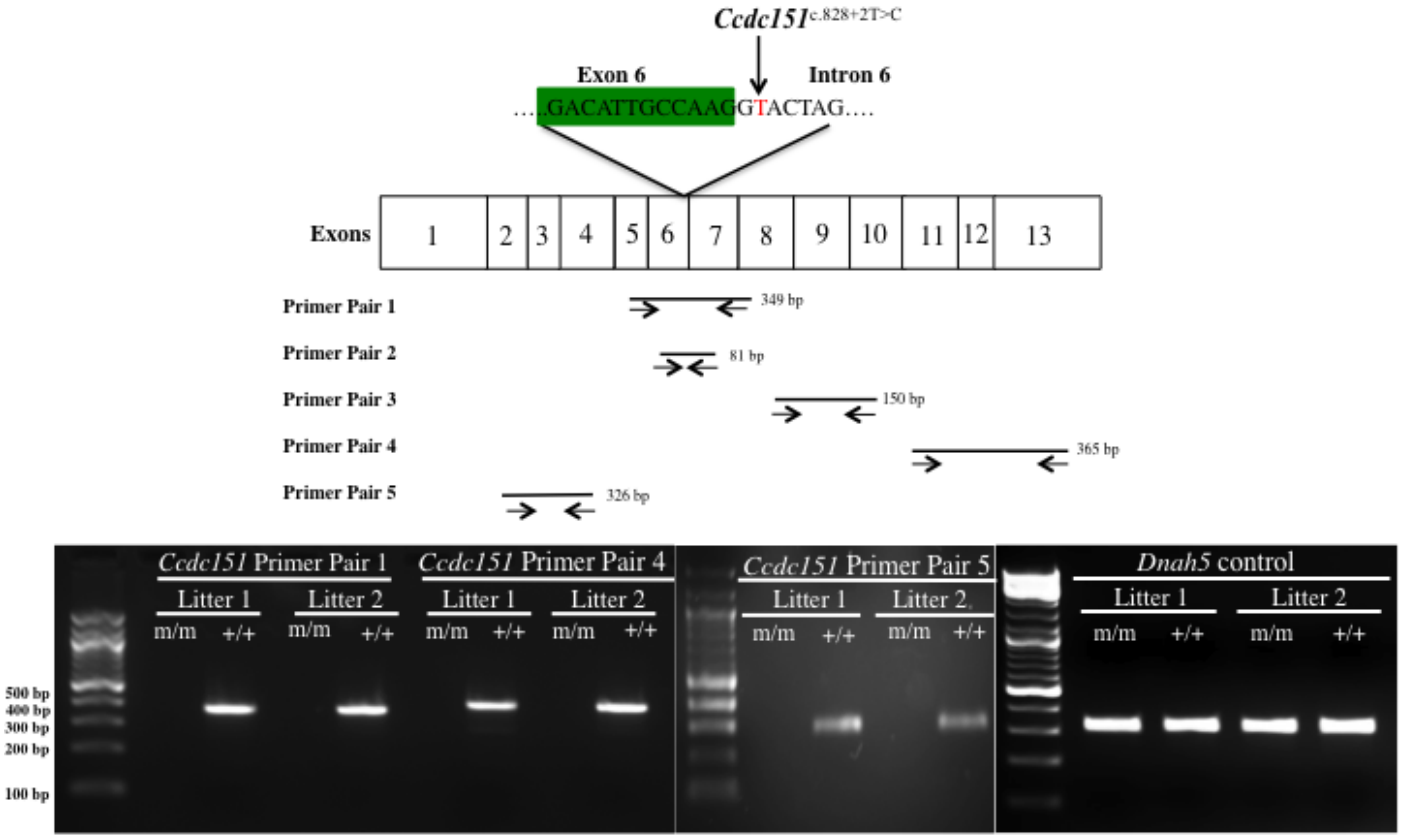


**Figure S5. RT-PCR confirmation of splice defect in *Ccdc151*$^{snbl}$ mice**. Total RNA was isolated from trachea of *Ccdc151*$^{snbl}$ mice and control littermates using the RNeasy Plus Micro Kit (Qiagen). cDNA was synthesized from total RNA and PCR amplified using AmpliTaq Gold™ DNA polymerase (Life Technologies) using cycle parameters: 95°C for 5 min, followed by 40 cycles at 95°C for 30 s, 58°C for 30 s and 72°C for 1 min, then 72°C for 5 min. Five primer pairs were used for PCR amplification to interrogate the *Ccdc151* transcript, and *Dnah5* was also amplified as a positive control (All primers listed in Table S1).

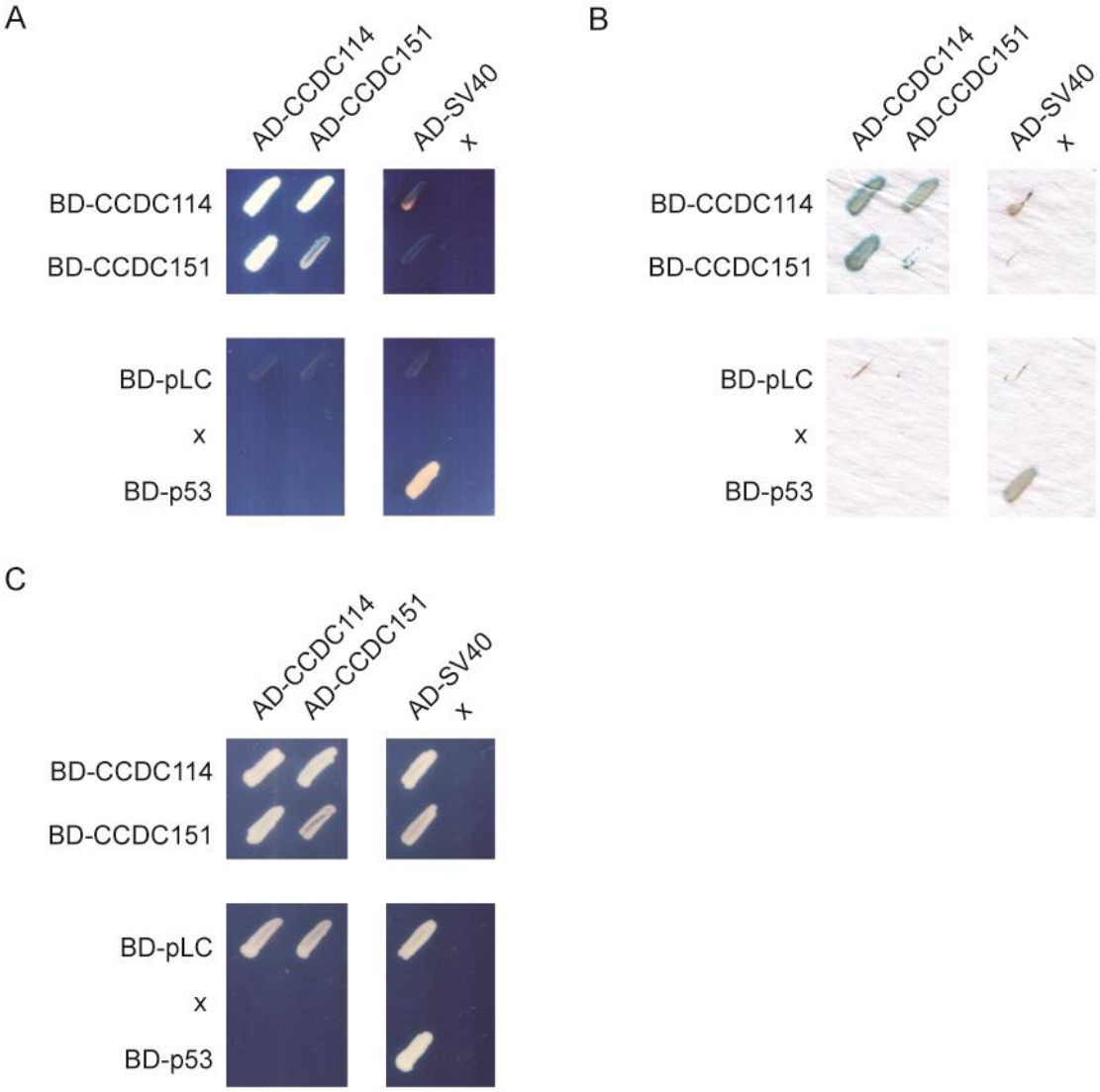


**Figure S6. Binary interaction between CCDC151 and CCDC114.** Yeast two-hybrid screening of CCDC151 and CCDC114 reveals direct protein interaction between CCDC151 and CCDC114. Plasmids expressing full-length CCDC151 and CCDC114 were fused to a DNA-binding domain (GAL4-BD) or to an activation domain (GAL4-AD), transformed in yeast strains PJ69-4A and PJ69-4α respectively, and subsequently combined by yeast mating. Diploids containing both plasmids were selected in media lacking leucine and tryptophane (SD-LW; panel C). Interactions were analyzed by assessment of reporter gene (*HIS3* and *ADE2*) activation via growth on selective media (SD-LWAH; panel A) and β-galactosidase colorimetric filter lift assays (*LacZ* reporter gene; panel B). As a positive control, the binding capacity of BD-p53 and SV40-AD was assessed; as negative controls, BD-pLC and AD-SV40, which thus far have not been associated with either CCDC151 or CCDC114, were included in this assay.

**Table S1. Miscellaneous primers used in this study**

| | **Forward** | **Reverse** |
|---|---|---|
| ***Flanders*** | GGGACAGCATGCCAAACTTGCTTATAATCAATC | CTTGGCAGCATCCTTAGACAGATGAGC |
| **Schmidtea** | | |
| **dsRNA** | | |
| *Smed-ic2* | GGGAATTAATCATACCGAAG | CATCCCAATGTATGAATCTG |
| *Smed-ccdc151* | CGAACTAGCTAGAGATACGC | ACACAAACTTTCTTGACGTG |
| **qPCR** | | |
| *CCDC151* (probe*:* UPL143) | Ttggccaagttgacattgaa | Gacattgtgaagcggaatttt |
| *GAPDH* (probe*:* UPL68) | CATCAAAATTGTGGAGAGATGG | CCAGTTGAAGCCGGAATAAT |
| ***Ccdc151*$^{SnbI}$** | | |
| primer pair 1 | TGCGCAACCTGGAGAATCGGC | CTCCATACGCTCTGTCTGAA |
| primer pair 2 | AGTGAATCAAGAGGCTATAA | CGATCTCTGATCGCAGACTC |
| primer pair 3 | TAGTGCGCAGGTTCCTGGCG | CGTGGAGCCTCCGCTGGCTCA |
| primer pair 4 | TGATACGGTATTGGCAGGAA | TAAGATCTGCGCAACCTATT |
| primer pair 5 | GAGAGCTCCCAATGGAACAT | TCTTGGACCTCTGCCATCTC |
| *Dnah5* | TGAGCTTTAACACGTTAGACACG | TCAGACTGTTCTGTGCACCTG |
| **cDNA cloning** | | |
| *CCDC114*-UTR pDONR201-*CCDC114* | 5'UTR-F: GAGCGAGACCCTGTCTAGAAAAA<br>GGGGACAAGTTTGTACAAAAAAGCAGGCTTCatg gaaggggagaggcgggcctac | 3'UTR-R: GAACAGGAGATCAGGAGTCAGAG<br>GGGGACCACTTTGTACAAGAAAGCTGGGTTTAgcccc gggagtctttgctggtggag |
| *CCDC151*-UTR pDONR201-*CCDC151* | 5'UTR-F: TAACCCCTAGGGGCCTTCAGCCC<br>GGGGACAAGTTTGTACAAAAAAGCAGGCTTCatg acatctcctctgtgcagggcg | 3'UTR-R: GGTAACATTTATTGCGCAACTCTGAGGCC<br>GGGGACCACTTTGTACAAGAAAGCTGGGTTTAggacc tccgagagcgacggtgcttc |

For dsRNA synthesis the T7 polymerase promoter sequence (TAATACGACTCACTATAGGG) was attached to the 5'-ends of forward and reverse primers. UPL numbers correspond to Roche Universal Probe Library probe numbers that were used to validate knockdown efficiency.

**Table S2. Filtering process for gene variants identified through gene panel sequencing of UCL-65 II:8**

| | **UCL-65 II:8** |
|---|---|
| **Total variants in gene panel** | 5,378 |
| **Variants in MAF<0.01 in 1000 genomes** | 584 |
| | |
| **Heterozygous variants** | 392 |
| Heterozygous nonsynonymous, splice-site, or insertion/deletion variants | 59 |
| Genes with compound heterozygous variants | 4 (*MLL3, PCSK5, DCHS1, DNAH2*) |
| Of these, genes with compound heterozygous variants, and predicted to have motile ciliary functions | 1 (*DNAH2*); 3 heterozygous variants:<br>(1) rs149406306: c.11899C>T, p.Pro3967Ser (benign)<br>(2) c.3481C>A, p.Arg2738Gln (benign)<br>(3) rs7601298: c.6226T>C, p.Ser2076Pro (rare, probably damaging, 0.97) |
| | |
| **Homozygous variants** | 190 |
| Homozygous nonsynonymous, splice-site, or insertion/deletion variants | 13 autosomal homozygous (*DNAH3, WNT2B, STAB2, NCOR2, DPF3, KRTAP9-1, KDM6B, CCDC40, CCDC151, KLHL23, MAML3, WDR27, PDHA1*) plus 4 x-linked hemizygous (*GPR112, IL1RAPL1, MXRA5, ATRX*) |
| Of these, genes with homozygous ORF-located variants, and predicted to have motile ciliary functions | 3 homozygous variants (*DNAH3, CCDC40, CCDC151*):<br>(1) *DNAH3* rs138753702: c.9881T>A, p.Tyr3294Phe (rare, possibly damaging, 0.837)<br>(2) *CCDC40* rs10693712: c.3040-3041insCAC, p.Arg1014ThrArg (rare, in-frame single residue insertion, consequence unknown)<br>*(3) CCDC151* c.925G>T, p.309* (unique, stop-gain) |

MAF: Minor allele frequency; ORF: open reading frame. Variant pathogenic predictions were assessed according to GERP, PolyPhen2, SIFT, Condel; only the Polyphen2 score is displayed.

**Table S3. Filtering process for gene variants identified through exome sequencing of 71154 II:2**

| | **71154 II:2** |
|---|---|
| Total variants in exome | 31,964 |
| Homozygous variants located in 14 autozygous regions totalling 174 Mb* | 1,480 |
| Variants with MAF <0.01 in exome variant server database or dbSNP 139 | 156 |
| Splice-site, nonsynonymous or insertion-deletion variants | 57 |
| Variants in PCD candidate genes | 1 (*CCDC151* c.1256C>T, p.Ser409*) |

MAF: Minor allele frequency;
*Regions determined from combined SNP and exome data analysis of 71154 II:2 the proband and 71154 II:1 an unaffected sibling (shown in dark blue in Figure S1).

**Table S4. Documented clinical features of individuals carrying *CCDC151* mutations**

| ID | Homozygous mutations | Sex | Age at diagnosis | Origin | TEM findings | Situs inversus | Neonatal respiratory distress syndrome | NO | LM | Documented bronchiectasis | Recurrent respiratory tract infections, chronic cough, wheeze, bronchitis | Sinusitis, rhinorrhea, nasal | Otitis media (OM) and hearing problems |
|---|---|---|---|---|---|---|---|---|---|---|---|---|---|
| OP-675 | c.925G>T; p.Glu309* | M | 16 years | Egypt | ODA defect | Situs inversus, cardiac ventricular septal defect | Yes | ND | Static | Yes | Chronic wet cough | Chronic sinusitis, chronic nasal obstruction | Normal hearing |
| OP-1255 | c.925G>T; p.Glu309* | F | 10 weeks | Egypt | ODA defect | Situs inversus | Yes, persistent tachypnea and desaturation below 90% from 2 days old. | 9-11 ppb | Static | Yes | Recurrent respiratory tract infections | Nasal obstruction and chronic nasal secretions | Normal hearing |
| PCD-65 II:7 | c.925G>T; p.Glu309* | F | 1 year | Arabic-Bedouin | ODA defect | Dextrocardia, abdominal situs inversus | Yes | ND | Static | ND | Pneumonia, recurrent productive cough, wheezing, bronchitis. Asthma. | Chronic sinusitis | Conductive hearing loss, OM and effusions |
| PCD-65 II:8 | c.925G>T; p.Glu309* | M | 6 years | Arabic-Bedouin | ODA defect | Situs solitus | Yes, symptoms from birth | ND | Static | ND | Pneumonia, recurrent productive cough | | OM and effusions |
| 71154 II:2 | c.1256C>T; p.Ser419* | M | 12 years | Pakistan | ODA defect | Dextrocardia, abdominal situs inversus | No | ND | Static | infiltrate/atelectasis in x-ray | Recurrent respiratory symptoms presumed to be asthma | Nasal polyps, chronic pansinusitus, runny blocked nose | |

M: Male; F: Female; TEM: Transmission electron microscopy; ODA: Outer dynein arm; NO: Nitric oxide; ND: Not determined; LM: Light microscopy; CBF: Ciliary beat frequency

**Table S5. Recovery of Disease Causing *Ccdc151* Mutation in *Snowball* Mutant**

| | ***Snowball* mutant (1885-004-LA)** |
|---|---|
| **Average Coverage** | 51.8x |
| **Total variants** | 3,604 |
| **Novel coding variants** | 69 |
| **Novel homozygous coding variants** | 5<br>(1) *Ept1*: c.C356A, p.P119Q<br>(2) *Atn1*: c.C1345T, p.R449C<br>(3) *Epor*: c.A523G, p.T175A<br>(4) *Ccdc151:* c.828+2T>C<br>(5) *Plec*: c.G5074A, p.A1692T |
| **Homozygous among all *snowball* mutants** | 1 (*Ccdc151*$^{c.828+2T>C}$) |

**Table S6. Cardiac defects documented in a panel of homozygous *Ccdc151*$^{snbl}$ mutant mice**

| ID | Situs | Apex | Loop | Arch | Atria | OFT | Septal Defects | IVC | Van Praagh | Lung | Bronchial branching | Gut | Abdomen situs | Liver situs |
|---|---|---|---|---|---|---|---|---|---|---|---|---|---|---|
| 1 | HTX | Lev | D | Right | SS | Inv* | mVSD | Left | {S, D, S} | Norm (3R/2L) | Norm | Norm | Norm. L(st/Sp/P) | Norm (1R/2L) |
| 2 | HTX | Dex | L | Right | SI | Inv | mVSD | Dual | {I, L, I} | Inv (1R/3L) | Inv | Mal | Dsc. R(St/Sp) Mid (P) | Norm (1R/2L) |
| 3 | HTX | Lev | D | Left | SS | Norm | None | Right | {S, D, S} | Norm (3R/2L) | Norm | Norm | Inv. R(St/Sp/P) | Inv (2R/1L) |
| 4 | HTX | Dex | L | Right | ND | Inv | ND | Left | {I, L, I} | Inv (2R/3L) | ND | Norm | Inv. R(St/Sp/P) | RI (1L/1R) |
| 5 | HTX | Dex | L | Right | ND | Inv | ND | Dual | {I, L, I} | LI (1R/1L) | ND | Norm | Norm. L(St/Sp/P) | Nml (1R/2L) |
| 6 | SIT | Dex | L | Right | ND | Inv | ND | Left | {I, L, I} | Inv (2R/3L) | ND | Norm | Inv. R(St/Sp/P) | Inv (2R/1L) |
| 7 | SIT | Dex | L | Right | ND | Inv | ND | Left | {I, L, I} | Inv (2R/3L) | ND | Mal | Inv. R(St/Sp/P) | Inv (2R/1L) |
| 8 | SIT | Dex | L | Right | SI | Inv | None | Left | {I, L, I} | Inv (2R/3L) | Inv | Norm | Inv. R(St/Sp/P) | Inv (2R/1L) |
| 9 | SIT | Dex | L | Right | SI | Inv | None | Left | {I, L, I} | Inv (2R/3L) | Inv | Mal | Inv. R(St/Sp/P) | Inv (2R/1L) |
| 10 | SIT | Dex | L | Right | SI | Inv | None | Left | {I, L, I} | Inv (2R/3L) | Inv | Norm | Inv. R(St/Sp/P) | Inv (2R/1L) |
| 11 | SIT | Dex | L | Right | SI | Inv | None | Left | {I, L, I} | Inv (2R/3L) | Inv | Norm | Inv. R(St/Sp/P) | Inv (2R/1L) |
| 12 | SS | Lev | D | Left | ND | Norm | ND | Right | {S, D, S} | Norm (3R/2L) | ND | Norm | Norm. L(st/Sp/P) | Norm (1R/2L) |
| 13 | SS | Lev | D | Left | ND | Norm | ND | Right | {S, D, S} | Norm (3R/2L) | ND | Norm | Norm. L(st/Sp/P) | Norm (1R/2L) |
| 14 | SS | Lev | D | Left | ND | Norm | ND | Right | {S, D, S} | Norm (3R/2L) | ND | Norm | Norm. L(St/Sp/P) | Norm (1R/2L) |
| 15 | SS | Lev | D | Left | ND | Norm | ND | Right | {S, D, S} | Norm (3R/2L) | ND | Norm | Norm. L(St/Sp/P) | Norm (1R/2L) |

**Situs:** HTX: Heterotaxy; SIT: *Situs inversus totalis*; SS: *Situs solitus*; **Apex (heart apex):** Lev: Levocardia; Dex: Dextrocardia; **Loop (heart looping):** D: D Loop; L: L Loop; **Atria:** SS: *Situs solitus*; SI: *Situs inversus totalis*; **OFT (cardiac outflow tract):** Inv: Inverted positioning; Norm: Normal positioning; Inv*: affects the major aortopulmonary collateral arteries (MAPCA) – this sample is missing left pulmonary artery, supply to lungs comes from the aorta; **Septal Defects:** mVSD: muscular ventricular septal defect; **IVC:** position of inferior vena cava; **Van Praagh:** Cardiac anatomy classification using a 3-part series of letters describing malorientation of the atria, ventricles, and great vessels respectively[1]. In brief, {S, D, S} indicates normal anatomy and {I, L, I} indicates heterotaxy/situs inversus; **Lung:** Norm: Normal lobation; Inv: Inverted lobation; R/L denotes number of right/left lobes; **Bronchial branching:** Norm: Normal branching; Inv: Inverted branching; **Gut:** Norm: normal looping; Mal: malrotation of the intestines; **Abdomen situs:** Norm: situs solitus positioning; Inv: situs inversus positing; Dsc: discordant positioning; **Liver situs:** Norm: Normal lobation; Inv: Inverted; StSpP: stomach, spleen, pancreas, either left (L) or right side (R); Mid: midline;  lobation, R/L denotes number of right/left lobes.

**Video legends**

**Video S1. Videomicroscopy showing dysmotile cilia in the Kupffer's vesicle of *flanders* (*ts272a*) mutant zebrafish**

**Video S2. Videomicroscopy showing motile cilia in the Kupffer's vesicle of control *flanders* unaffected sibling**

**Video S3. Videomicroscopy showing pronephric ciliary beat in unaffected embryos**

**Video S4. Videomicroscopy showing pronepric ciliary beat in *flanders* mutant.** Cilia beat regularly with significantly reduced beat frequency.

**Videos S5-S6. *ccdc151* RNAi planarians move by muscle contraction rather than gliding**. Planarians were injected with dsRNAs either against gfp (control; **Video S5**) or *ccdc151* (**Video S6**). Videos were taken 14 days after the first dsRNA injection using a stereomicroscope (Leica M80 with Leica IC80 HD Camera).

**Video S7. Videomicroscopy showing immotile cilia in the tracheal epithelia of *Ccdc151*$^{Snbl}$ mutant**
Videomicroscopy of tracheal airway epithelia from homozygous *Ccdc151*$^{Snbl}$ mutant mice reveals immotile cilia, whereas littermate control mice show normal rapid synchronous ciliary beating.

**Video S8. Videomicroscopy showing motile cilia dysfunction in ependymal cilia of *Ccdc151*$^{Snbl}$ mutant**
Videomicroscopy of brain tissue sliced from the third ventricle of newborn homozygote *Ccdc151*$^{Snbl}$ mutant mice reveals mostly immotile cilia, with patches of cilia having slow and restricted ciliary motion. In contrast, ependymal cilia from littermate control mice show normal rapid synchronous ciliary beating.

**Video S9. Visualisation of an apparent coronary fistula in a *Ccdc151*$^{Snbl}$ mutant**
A digital video recording of a *Ccdc151*$^{Snbl}$ mutant shows the heart beating through its contractile cycle, with a coronary artery fistula delineating a longitudinal translucent dark red region in the ventricular septum (indicated by arrow). This was confirmed by histopathology examination (see **Figures 3D, VII, VIII and IX**).

**Video S10. Analysis of ciliary beating pattern of respiratory cilia from OP-675 by high-speed videomicroscopy.** The cilia are immotile.

**Video S11. Analysis of ciliary beating pattern of respiratory cilia from OP-1255 by high-speed videomicroscopy.** The cilia are immotile.

**Video S12. Analysis of ciliary beating pattern of respiratory cilia from a control by high-speed videomicroscopy.**

## Supplemental references


1. Schallert, E.K., Danton, G.H., Kardon, R., and Young, D.A.(2013). Radiographics *33*, 33-46.